bioRxiv preprint doi: https://doi.org/10.1101/2020.12.07.414607; this version posted December 7, 2020. The copyright holder for this preprint (which was not certified by peer review) is the author/funder, who has granted bioRxiv a license to display the preprint in perpetuity. It is made available under aCC-BY 4.0 International license.

Title: Rapid evolution of bacterial mutualism in the plant rhizosphere

Authors/ Affiliations

Erqin Li[1,2,3], Ronnie de Jonge[1,4,5*], Chen Liu[1], Henan Jiang[1], Ville-Petri Friman[6], Corné M.J. Pieterse[1], Peter A.H.M. Bakker[1*] and Alexandre Jousset[7*]

[1]Utrecht University, Department of Biology, Plant-Microbe Interactions, Padualaan 8, 3584 CH, Utrecht, The Netherlands.

[2]Freie Universität Berlin, Institut für Biologie, Altensteinstr. 6, D-14195 Berlin, Germany.

[3]Berlin-Brandenburg Institute of Advanced Biodiversity Research, D-14195 Berlin, Germany.

[4]VIB Center for Plant Systems Biology, Technologiepark 952, B-9052, Ghent, Belgium.

[5]Ghent University, Department of Plant Biotechnology and Bioinformatics, Technologiepark 952, B-9052, Ghent, Belgium.

[6]University of York, Department of Biology, Wentworth Way, YO10 5DD, York, United Kingdom.

[7]Utrecht University, Department of Biology, Ecology and Biodiversity, Padualaan 8, 3584 CH, Utrecht, The Netherlands.

Author List Footnotes

Further information and requests for resources and reagents should be directed to and will be fulfilled by the Lead Contact, Alexandre Jousset (A.L.C.Jousset@uu.nl).

*Correspondence to: A.L.C.Jousset@uu.nl, P.A.H.M.Bakker@uu.nl, r.dejonge@uu.nl

bioRxiv preprint doi: https://doi.org/10.1101/2020.12.07.414607; this version posted December 7, 2020. The copyright holder for this preprint (which was not certified by peer review) is the author/funder, who has granted bioRxiv a license to display the preprint in perpetuity. It is made available under aCC-BY 4.0 International license.

Summary

Even though beneficial plant-microbe interactions are commonly observed in nature, direct evidence for the evolution of bacterial mutualism in the rhizosphere remains elusive. Here we use experimental evolution to causally show that initially plant-antagonistic *Pseudomonas protegens* bacterium evolves into mutualists in the rhizosphere of *Arabidopsis thaliana* within six plant growth cycles (6 months). This evolutionary transition was accompanied with increased mutualist fitness via two mechanisms: *i)* improved competitiveness for root exudates and *ii)* enhanced capacity for activating the root-specific transcription factor gene *MYB72*, which triggers the production of plant-secreted scopoletin antimicrobial for which the mutualists evolved relatively higher tolerance to. Genetically, mutualism was predominantly associated with different mutations in the GacS/GacA two-component regulator system, which conferred high fitness benefits only in the presence of plants. Together, our results show that bacteria can rapidly evolve along the parasitism-mutualism continuum in the plant rhizosphere at an agriculturally relevant evolutionary timescale.

Keywords: experimental evolution, mutualism, plant-microbe interaction, diversification, rhizosphere, genetics

bioRxiv preprint doi: https://doi.org/10.1101/2020.12.07.414607; this version posted December 7, 2020. The copyright holder for this preprint (which was not certified by peer review) is the author/funder, who has granted bioRxiv a license to display the preprint in perpetuity. It is made available under aCC-BY 4.0 International license.

Introduction

Mutualistic interactions between multicellular hosts and their associated microbiota are important for the fitness of both parties [1–4]. However, while commonly observed in nature, direct evidence for the evolution of mutualism at both phenotypic and genotypic level is still scarce [5–7]. The rhizosphere is a hotspot for mutualistic interactions between the plant and free-living microorganisms. For example, plants can preferentially interact with mutualistic microbes present in the indigenous species pool of the soil and disproportionally increase their relative abundances in the rhizosphere [8–10]. While such plant-mediated ecological filtering can rapidly change the relative abundances of mutualistic versus antagonistic species in the rhizosphere, it is less clear if plants can drive evolution of mutualism within species by increasing the fitness of emerging *de novo* mutualist genotypes. For example, even the most well-known plant mutualistic microbes, nitrogen-fixing rhizobia [5] and phosphorus-providing mycorrhizae [11], can be detrimental to the plant, suggesting that the interaction between a given pair of plant and microorganism varies naturally [12,13]. It is thus possible that plant-associated microbes might evolve along the parasitism-mutualism continuum in response to selection exerted by plants.

Beneficial symbioses between eukaryotic and prokaryotic organisms have evolved multiple times across the eukaryotic domain [14] and are considered as one of the major evolutionary transitions of life [15]. It has been suggested that the evolution of mutualism often requires two basic components: currency and mechanism of exchange of the currency [14]. In the context of plant-bacteria interactions, currency could be, for example, a root exudate, which can be taken up by bacteria. Similarly, bacteria might produce plant growth-promoting hormones such as auxin and gibberellins [16], that are beneficial for plant growth. When the currency exchange between both parties is symmetrical, the selection is expected to favour the evolution of mutualism. Increased

bioRxiv preprint doi: https://doi.org/10.1101/2020.12.07.414607; this version posted December 7, 2020. The copyright holder for this preprint (which was not certified by peer review) is the author/funder, who has granted bioRxiv a license to display the preprint in perpetuity. It is made available under aCC-BY 4.0 International license.

mutualistic dependence is then thought to evolve via reciprocal coevolution or via adaptation by one of the partners via selection on traits that are directly involved in the mutualistic interaction [15]. However, currency exchange could also be asymmetrical, due to competition for shared limiting nutrients, such as iron [17], which could explain why certain plant-microbe interactions are antagonistic. Moreover, due to the open nature of the rhizosphere, free diffusion of plant-derived resources could select for increased levels of cheating where mutant bacterial genotypes take advantage of 'public goods' without contributing to the production of plant growth-promoting compounds [5,17]. As a result, mutualistic plant-microbe interactions might require additional enforcing from the plant [5] via sanctioning of cheating bacterial genotypes.

To assess whether plant-microbe mutualism can emerge as a consequence of plant-mediated effects, we used an *in vivo* experimental evolution design [18] where we allowed the rhizosphere bacterium *Pseudomonas protegens* CHA0 to evolve on the roots of *Arabidopsis thaliana* in the absence of other microbes. Furthermore, we used sterile sand free of organic carbon as the growth substrate making bacterial growth obligately dependent on plant root exudates. As a result, bacterial survival and evolution was solely dependent on the presence of the plant, and the performance of evolved bacterial selection lines were thus compared with the ancestral bacterial strain. To set up the selection experiment, we inoculated a clonal bacterial population on the roots of five independent *A. thaliana* Col-0 replicate plant selection lines and grew the plants and *P. protegens* in otherwise gnotobiotic conditions for a total of six plant growth cycles, which lasted four weeks each. At the end of every growth cycle, the evolved bacterial populations were isolated and transferred to the rhizosphere of new sterile plants (Fig. S1). In these experimental conditions, the initial plant-bacterium interaction was antagonistic: *A. thaliana* aboveground biomass was clearly reduced in the presence of *P. protegens* CHA0 after one growth cycle ($F_{1, 8} = 45.4$, $P < 0.001$, Fig. 1A), and likely cause for this is the production of diverse bioactive metabolites by

bioRxiv preprint doi: https://doi.org/10.1101/2020.12.07.414607; this version posted December 7, 2020. The copyright holder for this preprint (which was not certified by peer review) is the author/funder, who has granted bioRxiv a license to display the preprint in perpetuity. It is made available under aCC-BY 4.0 International license.

CHA0 [19] that can constrain plant growth [20]. To quantify changes in plant-bacterium interaction, sixteen evolved bacterial colonies were randomly selected from each plant replicate selection line at the end of the second, fourth and sixth growth cycles, in addition to sixteen randomly selected ancestral colonies (in total 256 isolates). Each isolated colony was characterized phenotypically by measuring multiple key life-history traits, including growth on different carbon sources and media, tolerance to diverse abiotic and biotic stresses, production of several bioactive compounds and their ability to inhibit other microorganisms (Table S1). A subset of bacterial phenotypes was also full genome sequenced and characterised for their effects on plant growth in terms of root architecture and above and belowground biomasses at the end of the selection experiment.

Results

Selection in the plant rhizosphere leads to bacterial phenotypic diversification and evolutionary transition towards mutualism

To study the evolution of *P. protegens* CHA0 in the *A. thaliana* rhizosphere, we isolated a total of 240 evolved bacterial isolates from every second time point along with sixteen ancestral isolates (Supplementary dataset 1) and used K-means clustering analysis to separate them into five distinct phenotypic groups based on measured all life-history traits (Fig. S2, Table S2). The phenotypic groups were then given names that reflected key differences in their appearance, life-history traits, and their mean effects on plant growth (Fig. 1; Fig. S3-S4). Evolved clones that clustered together with the ancestral strain were named as 'Ancestral-like' phenotype. Another phenotype similar to the ancestral strain, which only appeared momentarily before dropping below detection level was named as 'Transient' phenotype (Figs. 1-2). A third phenotype that resembled the ancestral strain, but which had clearly reduced abiotic stress tolerance ($F_{5, 248}$ = 40.8, P< 0.001, Fig. S4) and increased ability to form a biofilm ($F_{5, 249}$ = 196.8, P< 0.001, Fig. S4), was named as 'Stress-

bioRxiv preprint doi: https://doi.org/10.1101/2020.12.07.414607; this version posted December 7, 2020. The copyright holder for this preprint (which was not certified by peer review) is the author/funder, who has granted bioRxiv a license to display the preprint in perpetuity. It is made available under aCC-BY 4.0 International license.

109 sensitive' phenotype. Agar plate assays were used to determine the effect of the evolved
110 phenotypes on *A. thaliana* growth. While the 'Ancestral-like', 'Transient' and 'Stress-sensitive'
111 phenotypes showed neutral effects on plant biomass relative to plant-only control lines (Shoot
112 biomass, $F_{6, 26} = 8.01$, $P< 0.001$; Root biomass, $F_{6, 26} = 2.84$, $P= 0.029$, Fig. 1), they had a negative
113 effect on the plant root length (Root length, $F_{6, 26} = 10.01$, $P< 0.001$, Fig. 1E) and resulted in clear
114 bleaching of plants indicative of reduced chlorophyll activity similar to the ancestor (the amount
115 of green pixels, $F_{6, 26} = 5.90$, $P< 0.001$, Fig. 1F). These assays also revealed two novel phenotypes
116 that showed positive effects on plant shoot and root biomasses (Fig. 1B, C) with comparable levels
117 of plant 'greenness' to no-bacteria control treatment (Fig. 1F). These evolved phenotypes were
118 therefore named as 'Mutualist 1' and 'Mutualist 2'as indicated by their plant growth-promoting
119 activity.

120 The relative abundance of different phenotype groups changed over time (Fig. 2A). The
121 'Ancestral-like' phenotypes persisted throughout the experiment even though they were substituted
122 by evolved phenotypes in all plant selection lines (Fig. 2A). The evolutionary success of 'Transient'
123 and 'Stress-sensitive' phenotypes was short-lived: 'Transient' phenotypes disappeared below the
124 detection limit in all plant selection lines by the end of the sixth growth cycle (Fig. 2A), while the
125 'Stress-sensitive' phenotypes emerged only in three selection lines and survived until the end of
126 the experiment only in one of the selection lines (Fig. 2A). In contrast, the frequency of mutualistic
127 phenotypes increased in four out of five plant selection lines throughout the experiment, while one
128 selection line became dominated by 'Ancestral-like' and 'Stress-sensitive' phenotypes (Fig. 2A).

129 An aggregated 'plant performance' index summarising the effects of each bacterial isolate
130 on both aboveground and belowground plant growth traits (Fig. 2B, PC1 of multivariate analysis),
131 was used to explore if reduced antagonism towards the plant was associated with improved
132 bacterial growth indicative of the evolution of reciprocally beneficial mutualistic interaction. We

bioRxiv preprint doi: https://doi.org/10.1101/2020.12.07.414607; this version posted December 7, 2020. The copyright holder for this preprint (which was not certified by peer review) is the author/funder, who has granted bioRxiv a license to display the preprint in perpetuity. It is made available under aCC-BY 4.0 International license.

133 found a significant positive correlation between plant performance index and bacterial phenotype
134 abundance per plant ($F_{1, 28} = 8.01$, $P < 0.001$, Fig. 2C). Specifically, both mutualistic phenotypes
135 reached higher abundances in the plant rhizosphere compared to other phenotypes (bacterial cells
136 per plant). This indicates that reduced bacterial antagonism towards the plant was coupled with
137 improved growth in the rhizosphere, which could also explain why mutualists became the dominant
138 phenotypes in four out of five plant selection lines during the selection experiment (reaching up to
139 94% relative abundance, Fig. 2A). In support for this, a similar positive correlation was observed
140 between the degree of plant performance of each phenotype measured in separate plant growth
141 assays and their relative abundance in diversified rhizosphere populations at the end of the selection
142 experiment ($F_{1, 23} = 4.37$, $P = 0.048$, Fig. S5). Together, these results demonstrate that the evolution
143 of plant-growth promotion was accompanied with increased bacterial fitness, indicative of a
144 mutualistic interaction where each species had a net benefit. As this evolutionary transition was
145 observed parallel in four out of five selection lines, it was likely driven by deterministic processes
146 such as selection exerted by the plant instead of random genetic drift due to bottlenecking between
147 plant growth cycles.
148
149 ***Evolution of mutualism is linked to improved resource catabolism and tolerance to plant-***
150 ***secreted antimicrobials***
151 For stable mutualism to evolve, plants would need to provide the evolved mutualists a 'currency'
152 that could not be accessed by the other phenotypes or employ some form of 'sanctioning' to
153 constrain the growth of non-mutualist phenotypes. To study this, we first compared differences in
154 the evolved phenotypes' ability to use a range of carbon sources that are typically found in *A.*
155 *thaliana* root exudates [21], and which could have selectively preferred the growth of mutualist
156 phenotypes. Second, we compared the evolved phenotypes' tolerance to scopoletin, which is an

bioRxiv preprint doi: https://doi.org/10.1101/2020.12.07.414607; this version posted December 7, 2020. The copyright holder for this preprint (which was not certified by peer review) is the author/funder, who has granted bioRxiv a license to display the preprint in perpetuity. It is made available under aCC-BY 4.0 International license.

157 antimicrobial secreted by plant roots known to modulate root microbiome composition for example
158 by favouring more tolerant bacterial taxa [22,23]. We found that the 'Mutualist 1' phenotype showed
159 an improved ability to grow on various different carbon sources compared to the other phenotypes
160 (PC1 of multivariate analysis, $F_{5, 248} = 50.72$, $P < 0.001$, Fig. 3A). This suggests that 'Mutualist 1'
161 potentially evolved an ability to compete better for plant-derived root exudates during the selection
162 experiment, which could have increased their abundance relative to other phenotypes. Moreover,
163 'Transient', 'Stress-sensitive' and 'Mutualist 2' phenotypes showed reduced growth on carbon
164 sources relative to 'ancestral-like' phenotypes indicative of competitive disadvantage (Fig. 3A).
165 To explore the potential significance of scopoletin, we used a GUS reporter assay to determine how
166 different bacterial phenotypes affected the expression of the plant root-specific gene *MYB72* [24],
167 which encodes a transcription factor that regulates the production of scopoletin. We found that
168 plants inoculated with 'Mutualist 1' and 'Mutualist 2' phenotypes retained high GUS activity,
169 which was comparable to the ancestor ($F_{5, 24} = 5.6$, $P < 0.01$, Fig. 3B, Fig. S6). However, the other
170 evolved phenotypes induced a reduced GUS activity in plant relative to the mutualists (Fig. 3B,
171 Fig. S6). While the 'Mutualist 1' and 'Mutualist 2' phenotype groups included strains that showed
172 very high tolerance to scopoletin, their mean tolerance did not significantly differ from other
173 phenotype groups ($F_{5, 24} = 1.76$, $P = 0.16$; Fig. 3C). However, a significant positive correlation was
174 observed between the induction of *MYB72* in *A. thaliana* roots and phenotypes' tolerance to
175 scopoletin ($F_{1, 28} = 8.29$, $P < 0.01$, Fig. 3D). This suggest that both the activation of scopoletin
176 production, and the scopoletin tolerance, were potentially under co-selection as mutualistic
177 phenotypes showed high scopoletin tolerance only when they were able to trigger increased
178 scopoletin production by the plant (upregulation of *MYB72*). Such mechanisms would have ensured
179 positive selection for mutualists relative to other evolved phenotypes.
180

bioRxiv preprint doi: https://doi.org/10.1101/2020.12.07.414607; this version posted December 7, 2020. The copyright holder for this preprint (which was not certified by peer review) is the author/funder, who has granted bioRxiv a license to display the preprint in perpetuity. It is made available under aCC-BY 4.0 International license.

Mutualistic phenotypes had mutations in genes encoding the GacS/GacA two-component regulatory system

To gain insights into the genetic mechanisms underlying the evolution of mutualism, we performed whole-genome re-sequencing of a subset of evolved isolates followed by reference-based identification of point mutations (SNPs) and insertions or deletions (INDELs). These analyses revealed that different evolved bacterial phenotypes were associated with relatively few mutations in global regulator genes (Fig. 4) underpinning their central role in bacterial adaptation [25,26]. While only few non-parallel mutations were observed in case of 'Ancestral-like' and 'Transient' phenotypes (Table S2), all but two mutualistic isolates (8/10) harboured mutations in genes encoding the GacS/GacA two-component system, which regulates secondary metabolism alongside many other aspects of bacterial physiology [27]. Despite high level of parallelism, a variety of different mutations was observed in this locus. Three *gacS*/*gacA* mutations were unique to 'Mutualist 1' isolates, and specifically associated with an uncharacterized N-terminal histidine kinase domain in GacS (G27D) and the response regulatory domain of GacA (G97S; D49Y, Fig. 4). Four unique 'Mutualist 2' mutations were found upstream (at -40 of the transcription start site) or inside the *gacA* coding region (E38*, D54Y and Y183S, Fig. 4). The conserved phosphate-accepting aspartate 54 (D54) residue is important for phospho-relay initiated by the sensor kinase GacS, and mutations of this residue are associated with complete loss-of-function [28–30]. Aspartate 49 (D49) is another conserved residue in the vicinity of D54, and the *gacA* (49Y) allele has previously been reported to be associated with a partial reduction in GacA activity [30]. The other mutations in *gacA* are novel and conceivably have a significant impact on GacA activity as they result in a severely truncated protein (E38*) or are located within the third recognition helix of the LuxR-like tetra-helical helix-turn-helix (HTH) domain, which is known to make most of the DNA contacts (Y183S) [31]. In line with the predicted effects of the mutations, 'Mutualist 1' isolates

bioRxiv preprint doi: https://doi.org/10.1101/2020.12.07.414607; this version posted December 7, 2020. The copyright holder for this preprint (which was not certified by peer review) is the author/funder, who has granted bioRxiv a license to display the preprint in perpetuity. It is made available under aCC-BY 4.0 International license.

retained part of the GacS/GacA – mediated traits, while 'Mutualist 2' isolates showed a severe to complete disruption of secondary metabolite production (Fig. S3). These differences between individual mutations are thus likely to explain the variation in life-history traits within and between the 'Mutualist 1' and 'Mutualist 2' phenotype groups.

Several other genes were also mutated in the mutualistic isolates, including *accC* (E413K) that encodes the biotin decarboxylase subunit of the acetyl coenzyme A carboxylase complex involved in fatty acid biosynthesis in bacteria, and *fleQ* (R320Q) which is linked with motility and biofilm formation (Fig. 4). These mutations were plant replicate line-specific, and their effect on bacterial physiology or bacteria-plant interactions are unknown. Interestingly, mutualists evolved in all except one selection line, which became dominated by 'Stress-sensitive' bacteria (Fig. 1, Fig. 4), that also transiently appeared in two other plant selection lines. Genetically, this phenotype was mainly associated with mutations in the *rpoS* coding region and its promoter (Q65*, 3/5 of selection lines). The *rpoS* gene encodes sigma factor *sigma-38*, which mediates general stress resistance [32,33], downregulates the biosynthesis of antagonistic secondary metabolites [34] and is involved in biofilm formation [35] with several bacteria. In line with this, we found that 'Stress-sensitive' phenotypes were able to form high amounts of biofilm *in vitro* (Fig. S4), which may have supported more efficient root colonization [36] and explain their dominance in one of the plant selection lines. Moreover, efficient root colonisation could have initiated a strong priority effect [37,38], potentially constraining the subsequent emergence of mutualistic bacterial phenotypes. One of the sequenced 'Stress-sensitive' clones had also a mutation in a TetR-family transcriptional regulator (*tetR*), indicative of generalised stress tolerance evolution. Together, these results show that plant selection can lead to high level of parallel evolution both at the phenotypic and molecular level.

The fitness benefits of GacS/GacA mutations are specific to the rhizosphere environment

bioRxiv preprint doi: https://doi.org/10.1101/2020.12.07.414607; this version posted December 7, 2020. The copyright holder for this preprint (which was not certified by peer review) is the author/funder, who has granted bioRxiv a license to display the preprint in perpetuity. It is made available under aCC-BY 4.0 International license.

In order to assess whether the observed mutations specifically conferred an advantage in the rhizosphere environment, we compared the fitness of evolved mutualists on plant roots and on liquid growth culture media. To this end, the fitness of two evolved *gacA* (Mutualists 1 and 2; ID 242 and ID 220, respectively, Table S2), and one *gacS* genotype (Mutualist 1, ID 222, Table S2) was compared relative to their direct ancestral genotypes without *gac* mutations (ID 133, ID 28 and ID 66, respectively, Table S2) within the same plant selection lines. Fitness was determined as the relative competitive fitness in direct pairwise competitions as a deviation from the initial 1:1 ancestor-to-successor ratio *in vivo* on *A. thaliana* roots and *in vitro* in Kings' B (KB), lysogeny broth (LB), and tryptic soy broth (TSB) growth media. Post-competitive genotype ratios were determined using PCR-based high-resolution melting profile (RQ-HRM) analysis (see Methods and Materials and Supplementary figure 7). It was found that all three *gacS/gacA* mutants had a higher fitness in the rhizosphere relative to their direct ancestral genotypes without *gac* mutations ($F_{3, 32} = 10.03$, $P < 0.001$, Fig. 5). Interestingly, this advantage was smaller for one of the *gacA* mutants (ID 220, $F_{2, 6} = 15.35$, $P = 0.004$, Fig. 5) likely because its direct ancestor already showed mutualistic behaviour due to a mutation in the *accC* gene, which likely reduced the relative benefit of the *gacA* mutation within this lineage (Table S2). While the fitness benefits of *gac* mutations were mainly observed in the rhizosphere, two *gac* mutants showed improved competitive fitness in KB media indicative of general metabolic adaptations (genotype × measurement environment: $F_{6, 24} = 13.02$, $P < 0.001$; genotype comparisons in KB media: $F_{2, 6} = 162.6$, $P < 0.001$). Together, these results confirm that the genetic changes underlying the evolution of bacterial mutualism were primarily driven by plant selection.

Discussion

bioRxiv preprint doi: https://doi.org/10.1101/2020.12.07.414607; this version posted December 7, 2020. The copyright holder for this preprint (which was not certified by peer review) is the author/funder, who has granted bioRxiv a license to display the preprint in perpetuity. It is made available under aCC-BY 4.0 International license.

Even though beneficial plant-microbe interactions are widely documented, their evolutionary origin is less well understood. Here we studied how an initially antagonistic relationship between *P. protegens* CHA0 bacterium and its host plant, *Arabidopsis thaliana*, changed during prolonged selection over six plant growth cycles (6 months). While several studies have previously reported beneficial effects of CHA0 strain on plant growth in natural soils, it initially showed antagonism towards the plant in our experimental conditions potentially due to production of phytotoxic compounds. Crucially, this interaction rapidly evolved during the experiment leading to clear phenotypic and genetic bacterial diversification and evolution of bacterial mutualists that had relatively higher competitive advantage in the rhizosphere, and positive effect on the plant growth compared to ancestral and other evolved bacterial phenotypes.

Based on our results, we suggest the following conceptual model for the evolution of mutualism. As bacterial growth in this system was dependent on plant root exudates, it is likely that reduction in the production of exoproducts, including lytic enzymes and antimicrobial secondary metabolites (Fig. S3), by mutualists had a positive effect on plant growth and the availability of plant-derived nutrients. As many metabolites produced by *Pseudomonas spp.* are potentially phytotoxic [20], the observed shift from antagonism to mutualism could therefore be explained by reduced toxicity to the plant. In turn, improved plant growth likely triggered selection for mutualists that were better at competing for root exudates relative to other phenotypes, or by selectively constraining the growth of non-mutualist phenotypes via certain sanctioning mechanisms. As a support for this, 'Mutualist 1' phenotypes evolved better at growing on plant-derived nutrients, while 'Mutualist 2' phenotypes evolved to activate plant-derived scopoletin production, a compound that was relatively more harmful to non-mutualistic phenotypes. Such differences between two mutualist phenotypes were also linked with subtle differences in the predicted functional effects of observed *gacS/gacA* mutations. Together, these adaptations could

bioRxiv preprint doi: https://doi.org/10.1101/2020.12.07.414607; this version posted December 7, 2020. The copyright holder for this preprint (which was not certified by peer review) is the author/funder, who has granted bioRxiv a license to display the preprint in perpetuity. It is made available under aCC-BY 4.0 International license.

have created a strong selective advantage for mutualistic phenotypes as evidenced by their relatively higher abundance in the rhizosphere at the end of the selection experiment.

At a genetic level, the evolution of mutualism could be achieved with only a few successive mutations involving mainly global regulators [29]. This result shows an interesting parallel with recent work demonstrating that the loss of a few virulence traits can turn a pathogen into a beneficial symbiont [7]. Evolution of mutualism was also linked with a clear phenotypic and genotypic bacterial diversification, which has previously been observed in aquatic [39] and soil [40] microcosms in response to spatial heterogeneity. Here we show that such bacterial diversification can also be driven by plant selection as evidenced by direct competition assays where competitive benefit observed in the rhizosphere was reduced or completely absent in lab media *in vitro*. Interestingly, we observed a contrasting evolutionary outcome in one of the five selection lines where 'Stress-sensitive' genotypes were able to become dominant alongside with 'Ancestral-like' genotypes potentially due to their enhanced ability to form biofilm and colonise plant roots. Interestingly, none of the phenotypes was able to reach fixation in the rhizosphere. One possibility for this is that the experiment was not long enough for the selective sweeps to drive beneficial mutations into fixation. Alternatively, it is possible that multiple phenotypes were able to coexist due to negative frequency dependent selection or because they occupied different spatial niches as seen in heterogenous soil environments [40,41]. These hypotheses could be studied directly in the future using fluorescent microscopy and tagged strains to observe diversification and genotype fluctuations in the rhizosphere both in space and time.

In summary, our results show that in addition to recruiting beneficial bacteria from multi-species microbial communities [8–10], plants could also change the functioning of its associated microbiota by creating strong selection for *de novo* evolution of mutualistic bacterial genotypes. Steering bacterial evolution in the rhizosphere could thus offer plants a shortcut to improve their

bioRxiv preprint doi: https://doi.org/10.1101/2020.12.07.414607; this version posted December 7, 2020. The copyright holder for this preprint (which was not certified by peer review) is the author/funder, who has granted bioRxiv a license to display the preprint in perpetuity. It is made available under aCC-BY 4.0 International license.

300 fitness without evolving themselves [42–44]. Future work should focus on validating our findings in
301 more complex microbial communities where bacterial diversification could be also affected by
302 interactions with other microbes. In conclusion, our results call for eco-evolutionary management
303 of plant-microbe interactions in agriculture by demonstrating that plant-associated bacteria can
304 rapidly evolve along the parasitism-mutualism continuum within a few plant growing seasons.

bioRxiv preprint doi: https://doi.org/10.1101/2020.12.07.414607; this version posted December 7, 2020. The copyright holder for this preprint (which was not certified by peer review) is the author/funder, who has granted bioRxiv a license to display the preprint in perpetuity. It is made available under aCC-BY 4.0 International license.

Figures

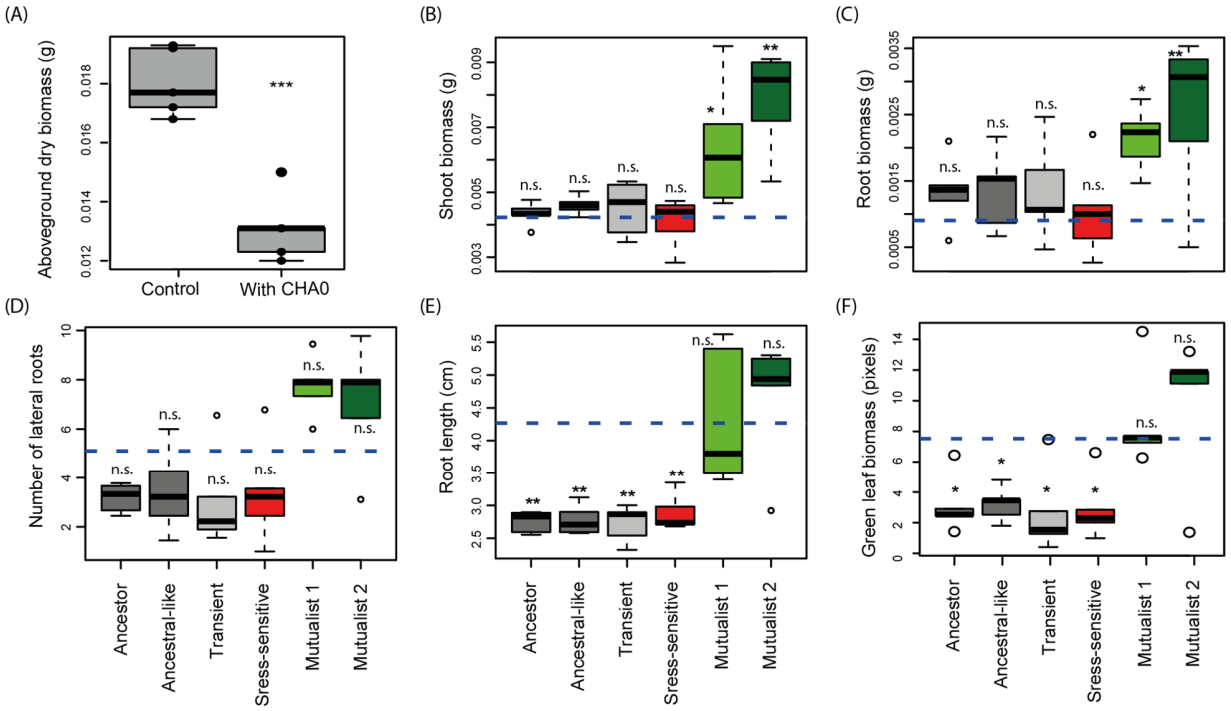

Figure 1. Evolution of bacterial mutualism in the rhizosphere of *Arabidopsis thaliana*. Panel (A) shows the initially antagonistic effect of *Pseudomonas protegens* CHA0 on *A. thaliana* after one plant growth cycle in the sterile sand study system. Panels (B-F) compare the effects of ancestral and evolved *Pseudomonas protegens* CHA0 phenotypes on plant performance-related traits in a separate plant growth assays performed on agar plates at the end of the selection experiment. Different panels show the shoot biomass in grams (B), root biomass in grams (C), number of lateral roots (D), root length in cm (E) and the amount of plant 'greenness' in terms of green-to-white pixel ratio (F) 14 days after bacterial inoculation (Supplementary dataset 2; blue dashed horizontal lines show the non-inoculated control plants). Bacterial phenotype groups are displayed as different colours and were classified and named based on K-means clustering (Figure S1) using 14 phenotypic traits linked to growth, stress tolerance, production of bioactive compounds, and antimicrobial activity (Table S1). Boxplots show the mean effect of five representative bacterial isolates from each evolved phenotype in addition to ancestor isolates (See Table S2). Statistical testing in all panels was carried out using ANOVA, and asterisks above plots indicate significant differences between control plants and bacteria-treated plants (*α=0.05, **α=0.01, ***α=0.001; n.s. = non-significant).

bioRxiv preprint doi: https://doi.org/10.1101/2020.12.07.414607; this version posted December 7, 2020. The copyright holder for this preprint (which was not certified by peer review) is the author/funder, who has granted bioRxiv a license to display the preprint in perpetuity. It is made available under aCC-BY 4.0 International license.

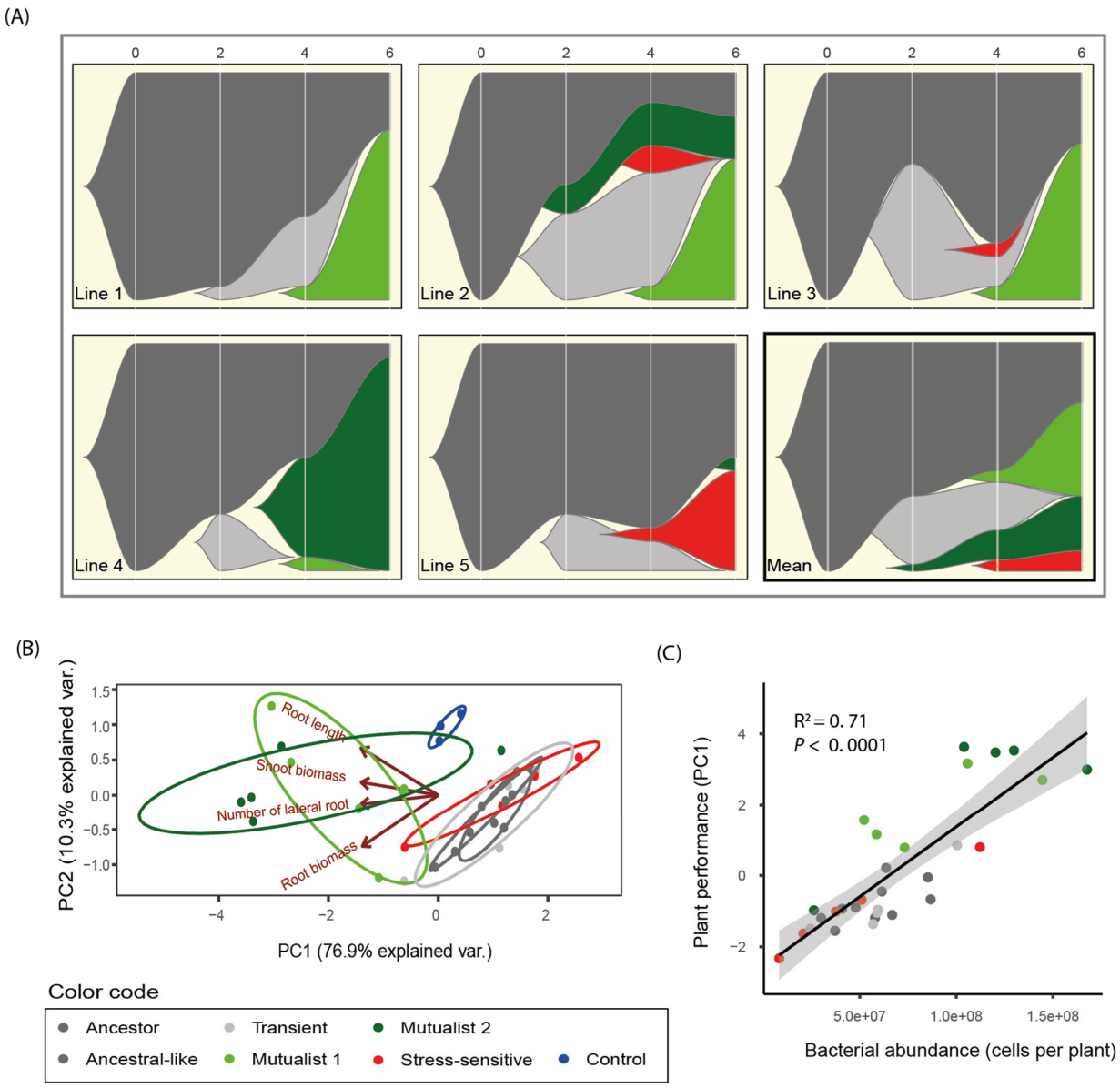

Figure 2. Temporal changes in bacterial phenotypes during the selection experiment and positive correlation between evolved bacteria and plant growth. Panels in A show the dynamics of five bacterial phenotype groups across five plant replicate lines and the overall mean pattern during six growth cycles (6 months). The x-axis shows the plant growth cycle (0: ancestral bacterium), and the y-axis shows the relative abundance of each bacterial phenotype. Panel (B) shows a principal component analysis (PCA) for five representative bacterial isolates from each

bioRxiv preprint doi: https://doi.org/10.1101/2020.12.07.414607; this version posted December 7, 2020. The copyright holder for this preprint (which was not certified by peer review) is the author/funder, who has granted bioRxiv a license to display the preprint in perpetuity. It is made available under aCC-BY 4.0 International license.

evolved phenotype group in addition to ancestor isolates (See Table S2) based on their plant growth-related traits. The negative PC1 values of each isolate were extracted and combined to a 'Plant performance' index, which included bacterial effects on shoot biomass, root biomass and root architecture explaining 76.9% of the total variation in plant growth. Panel (C) shows a positive correlation between 'Plant performance' and bacterial abundance in the plant roots at the end of the fitness assays.

bioRxiv preprint doi: https://doi.org/10.1101/2020.12.07.414607; this version posted December 7, 2020. The copyright holder for this preprint (which was not certified by peer review) is the author/funder, who has granted bioRxiv a license to display the preprint in perpetuity. It is made available under aCC-BY 4.0 International license.

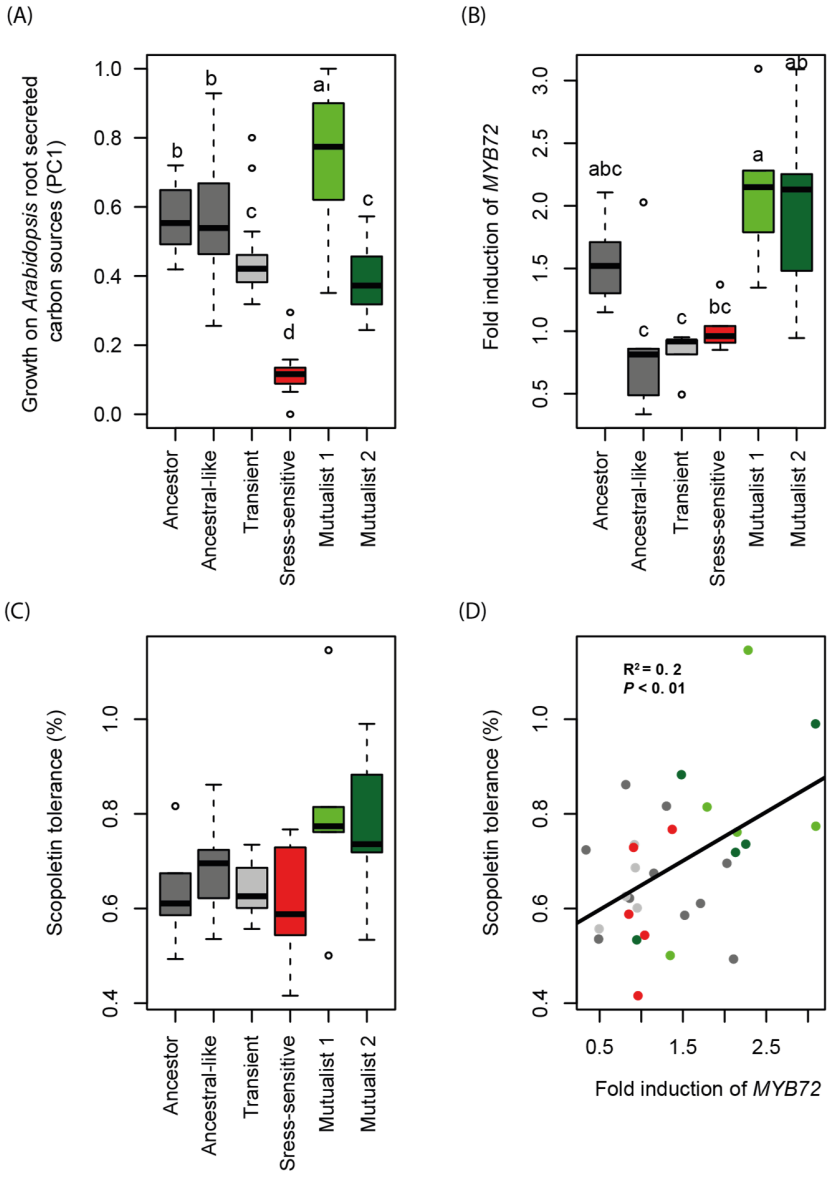

Figure 3. Selection mechanisms favouring the increase in the relative abundance of mutualists in the rhizosphere of *Arabidopsis thaliana*. Panel (A) shows the growth of ancestor and evolved *Pseudomonas protegens* CHA0 phenotypes on carbons typically secreted by *A. thaliana* (14 most dominant carbons analysed as a combined index based on normalised first principal component (PC1, which explained 83.9 % of total variation); in total, 16 ancestral, 119 'Ancestral-like', 11 'Stress-sensitive', 37 'Mutualist 1', 31 'Mutualist 2' and 41 'Transient' isolates

bioRxiv preprint doi: https://doi.org/10.1101/2020.12.07.414607; this version posted December 7, 2020. The copyright holder for this preprint (which was not certified by peer review) is the author/funder, who has granted bioRxiv a license to display the preprint in perpetuity. It is made available under aCC-BY 4.0 International license.

were characterized, Supplementary dataset 1). Panel (B) shows the effect of ancestor and evolved *P. protegens* CHA0 phenotypes on the expression of *MYB72* (transcription factor responsible for scopoletin production) in the roots of a GUS *A. thaliana* reporter line (based on the quantification of GUS staining of the roots, Fig. S6). Panel (C) shows the relative growth of ancestor and evolved *P. protegens* CHA0 phenotypes in the presence of the plant-secreted scopoletin antimicrobial at 2 mM concentration after 96 hrs of incubation relative to no-scopoletin control. Panel (D) shows a positive relationship between *MYB72* expression (fold induction; x-axis) and scopoletin tolerance (y-axis) for all tested isolates. Panels (B-D) include five representative bacterial isolates from each phenotype in addition to the ancestor (each replicate line represented; See Table S2). In all panels, colours represent different phenotype groups and statistical testing in panels (A-C) was carried out using ANOVA (different letters indicate significant differences based on a Tukey HSD test (α=0.05)).

bioRxiv preprint doi: https://doi.org/10.1101/2020.12.07.414607; this version posted December 7, 2020. The copyright holder for this preprint (which was not certified by peer review) is the author/funder, who has granted bioRxiv a license to display the preprint in perpetuity. It is made available under aCC-BY 4.0 International license.

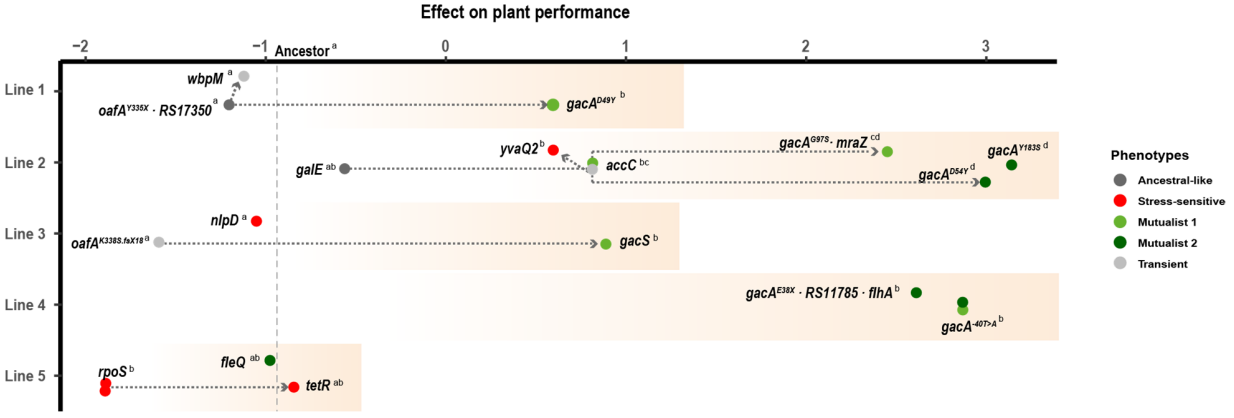

Bacterial phenotype	Plant replicate line	Mutation	Protein function
Mutualist 1	Line 1	*gacA* (D49Y)	Two-component regulator
	Line 2	*gacA* (Y97S)	Two-component regulator
		mraZ (upstream(221bp))	Transcriptional regulator MraZ
		accC (E413K)	Biotin carboxylase
	Line 3	*gacS* (G27D)	Two-component regulator
Mutualist 2	Line 2	*gacA* (Y183S)	Two-component regulator
		gacA (D54Y)	Two-component regulator
	Line 4	*gacA* (upstream (40 bp))	Two-component regulator
		gacA (E38X)	Two-component regulator
		RS11785 (S256C)	LysR family transcriptional regulator
		flhA (H393Q.fsX15)	Flagellar biosynthesis protein FlhA
	Line 5	*fleQ* (R320Q)	Sigma-54-dependent Fis family transcriptional regulator
Stress-sensitive	Line 2	*yvaQ2* (upstream (9 bp))	Methyl-accepting chemotaxis protein
	Line 3	*nlpD* (Q197P)	LysM, promotor for *rpoS*
	Line 5	*rpoS* (Q65X)	Sigma-38, stress regulon
		tetR (Y127X)	TetR family transcriptional regulator

Figure 4. Genetic basis of bacterial evolution in the rhizosphere of *Arabidopsis thaliana*. Clear parallel evolution was observed between four out five plant replicate selection lines based on re-sequencing of 25 evolved and five ancestor isolates used in the phenotypic assays. Filled dots represent isolates with non-synonymous mutations (present in 18/25 evolved isolates), and the x-axis shows a combined index of 'Plant performance' relative to non-inoculated control plants (values on the x-axis indicate positive and negative effects on the plant and the y-axis shows the five independent plant replicate selection lines). The effect of the ancestral bacterial genotype on plant performance is shown as a vertical dashed line. The different letters on the top right of each

bioRxiv preprint doi: https://doi.org/10.1101/2020.12.07.414607; this version posted December 7, 2020. The copyright holder for this preprint (which was not certified by peer review) is the author/funder, who has granted bioRxiv a license to display the preprint in perpetuity. It is made available under aCC-BY 4.0 International license.

375 genotype indicate significant differences based on a Tukey HSD test (α=0.05; each line analysed
376 separately). The accumulation of mutations within replicate lines are shown with connected dashed
377 arrows. The table lists unique mutations (and the strains' ID number) linked with evolved bacterial
378 phenotypes, and additional mutations that appeared later during the experiment within the same
379 genetic background are shown after the indent; notably, these additional mutations did not affect
380 the bacterial phenotypes (See Table S3 for a more detailed description of the mutations).

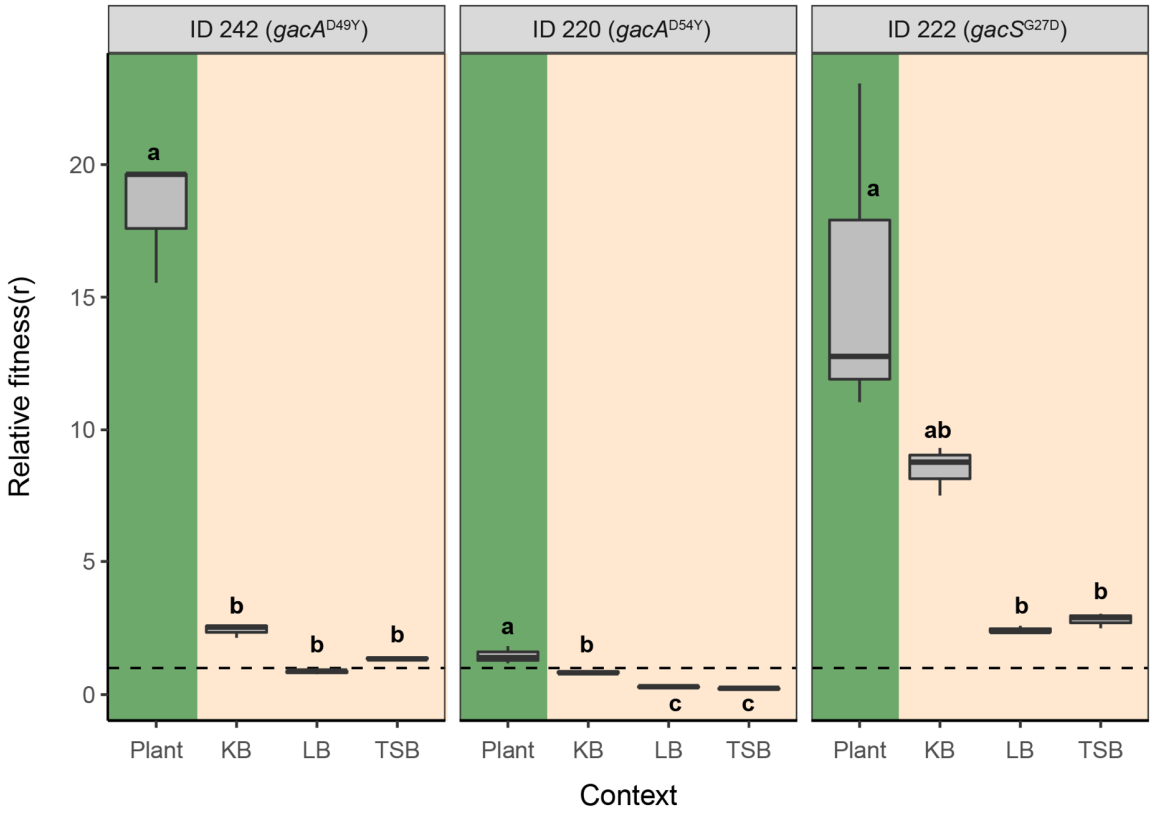

381

382 **Figure 5. Competitive fitness of *gac* mutants relative to their direct ancestors in the**
383 **rhizosphere and in *in vitro* culture media.** The *gac* mutants' relative fitness (*r*) was calculated
384 based on the deviation from the initial 1:1 genotype ratio (dashed line) after direct competition in
385 different environments. Fitness values above the dashed line indicate a relatively higher
386 competitive advantage of *gac* mutants relative to their ancestral genotypes without *gac* mutations

bioRxiv preprint doi: https://doi.org/10.1101/2020.12.07.414607; this version posted December 7, 2020. The copyright holder for this preprint (which was not certified by peer review) is the author/funder, who has granted bioRxiv a license to display the preprint in perpetuity. It is made available under aCC-BY 4.0 International license.

(Table S2), whereas values below the dashed line denote for decreased competitive ability of evolved *gac* mutants. In all panels, green and beige backgrounds denote competition assays conducted in the rhizosphere and in standard culture media, respectively. Different small letters above the boxplots represent significant differences in *r* between growth conditions for each mutant based on three biological replicates (one-way ANOVA, Tukey's HSD test, α=0.05).

bioRxiv preprint doi: https://doi.org/10.1101/2020.12.07.414607; this version posted December 7, 2020. The copyright holder for this preprint (which was not certified by peer review) is the author/funder, who has granted bioRxiv a license to display the preprint in perpetuity. It is made available under aCC-BY 4.0 International license.

Materials and Methods

Bacterial strain and growth conditions

We used *Pseudomonas protegens* (formerly *Pseudomonas fluorescens*) [45] CHA0 as a model strain, which was initially isolated from tobacco roots [46]. The strain was chromosomally tagged with GFP and a kanamycin resistance cassette to enable specific tracking of the strain and detection of contaminations [19]. This bacterium has the genetic potential to produce various bioactive metabolites, including the plant hormone indole-3-acetic acid (IAA), antimicrobial compounds and lytic enzymes [47]. Prior to the experiment, bacteria were grown for 48 h on a King's medium B [48] (KB) agar plate supplemented with 50 µg ml^{-1} kanamycin, a single colony was randomly picked and grown for 12 h in KB at 28 °C with agitation. The cell culture was then washed for three times in 10 mM $MgSO_4$ and adjusted to 10^7 cells ml^{-1} and used as inoculant for all plants. This inoculant was also stored at -80 °C as frozen ancestral stock, from which 'Ancestor' isolates were picked in later experiments.

Host plant and growth conditions

We used *Arabidopsis thaliana* ecotype Col-0 as a model host plant. Surface-sterilized seeds were first sown in Petri dishes with agar-solidified (1.5% agar (w/v)) modified Hoagland's medium: (KNO_3 (3 mM), $MgSO_4$ (0.5 mM), $CaCl_2$ (1.5 mM), K_2SO_4 (1.5 mM), NaH_2PO_4 (1.5 mM), H_3BO_3 (25 µM), $MnSO_4$ (1 µM), $ZnSO_4$ (0.5 µM), $(NH_4)_6Mo_7O_{24}$ (0.05 µM), $CuSO_4$ (0.3 µM), MES (2.5 mM) and 50 µM Fe(III)EDTA, pH = 5.8) and stratified for 2 days at 4 °C after Petri dishes were positioned vertically and transferred to a growth chamber (20 °C, 10 h light/14 h dark, light intensity 100 µmol m^{-2} sec^{-1}). After two weeks of incubation, two seedlings were transferred to

bioRxiv preprint doi: https://doi.org/10.1101/2020.12.07.414607; this version posted December 7, 2020. The copyright holder for this preprint (which was not certified by peer review) is the author/funder, who has granted bioRxiv a license to display the preprint in perpetuity. It is made available under aCC-BY 4.0 International license.

415 closed and sterile ECO2 boxes (http://www.eco2box.com/ov80xxl_nl.htm) for selection
416 experiment. The ECO2 boxes were filled with 260 g of dry, carbon-free silver sand that was
417 previously washed with MilliQ water to remove dissolvable chemical elements and heated to 550
418 °C for 24 h to remove remaining organic material. Prior to transplantation the sand was amended
419 with 13 ml of modified Hoagland medium.
420

421 **Design of the selection experiment**

422 The selection experiment was conducted in a gnotobiotic system to remove confounding effects
423 that may emerge as a result of competitive interactions with other micro-organisms, and to place
424 the focus on plant-mediated selective pressures. Moreover, we allowed only the bacteria to evolve
425 during the experiment and used new clonal plants at every bacterial transfer. We set up five
426 independent plant-bacterium replicate lines, which were grown for six independent plant growth
427 cycles (see Figure S1 for an overview of the experimental design). The experiment was started by
428 inoculating 10^6 cells of the stock *P. protegens* CHA0 culture (From here on abbreviated as
429 "ancestor") into the rhizosphere of two-week-old *A. thaliana* seedlings growing in sterile silver
430 sand within ECO2 boxes (two plants per replicate selection line). Inoculated plants were then
431 grown for four weeks (20 °C, 10 h light/14 h dark, light intensity 100 µmol m^{-2} sec^{-1}) after which
432 the plant growth cycle was terminated and root-associated bacteria were harvested by placing the
433 roots of both plants into a 1.5 ml Eppendorf tubes filled with 1 ml 10 mM $MgSO_4$ and two glass
434 beads. Rhizosphere bacteria were suspended into the liquid using TissueLyser II at a frequency of
435 20 s^{-1} for 1 min after which bacterial cell densities were determined using flow cytometry (BD
436 Accuri™ C6 Plus, thresholds for FSC: 2000, SSC: 8000). After this, 10^6 cells were inoculated to
437 the rhizosphere of new *A. thaliana* plants to initiate the next plant growth cycle. Possible

bioRxiv preprint doi: https://doi.org/10.1101/2020.12.07.414607; this version posted December 7, 2020. The copyright holder for this preprint (which was not certified by peer review) is the author/funder, who has granted bioRxiv a license to display the preprint in perpetuity. It is made available under aCC-BY 4.0 International license.

438 contaminations were checked by plating the suspension on 3 g l^{-1} tryptic soy agar (TSA) plates and
439 it was verified that all colonies carried the *GFP* marker gene, as observed under UV light.
440

441 ## Bacterial life-history traits measurements

442 Individual bacterial colonies were isolated from all replicate plant selection lines for life-history
443 measurements at the end of the second, fourth and sixth plant growth cycle by dilution plating the
444 rhizosphere suspension on 3 g l^{-1} TSA plates. After incubation at 28 °C for 24 h, 16 colonies were
445 randomly picked from each replicate selection lines resulting in a total of 240 evolved and 16
446 ancestral colonies. All these colonies were characterized for a set of key bacterial life-history traits
447 representative of growth, stress resistance and traits linked with plant-microbe interactions.

448 ***a. Bacterial growth yield in KB medium***

449 All the bacterial isolates were grown in 96-well plates with 160 µl 1/3 strength liquid KB, at 20 °C
450 without shaking. Bacterial yield was determined as the maximum optical density at 600 nm after
451 three days of growth using a spectrophotometer (SPECTROstar Nano).

452 ***b. Bacterial stress resistance***

453 We measured bacterial resistance to a range of different stresses using various 96-well microplate
454 assays. Abiotic stress resistance was determined by growing bacteria in 160 µl of 1 g l^{-1} tryptic soy
455 broth (TSB) containing 0.0025% H_2O_2 (oxidative stress), 15% polyethylene glycol (PEG)-6000
456 (water potential stress) or 2% NaCl (salt stress). We used resistance to antibiotics commonly
457 produced by rhizosphere microorganisms as indicator of biotic stress resistance. Antibiotic
458 resistance was tested in 160 µl of 1 g l^{-1} TSB supplemented with 1 µg ml^{-1} streptomycin, 1 µg ml^{-1}
459 tetracycline, or 5 µg ml^{-1} penicillin, respectively. Bacterial growth with and without stresses were
460 determined after three days of growth at 20 °C without shaking as optical density at 600 nm and

bioRxiv preprint doi: https://doi.org/10.1101/2020.12.07.414607; this version posted December 7, 2020. The copyright holder for this preprint (which was not certified by peer review) is the author/funder, who has granted bioRxiv a license to display the preprint in perpetuity. It is made available under aCC-BY 4.0 International license.

stress resistance defined as the ratio of bacterial growth in the stressed relative to the non-stressed control treatment.

c. Traits linked with plant-microbe interactions

P. protegens CHA0 harbours several traits that are linked to plant growth including production of antibiotics and plant hormones. To assess these traits, we grew each bacterial colony in 96-well plates containing 160 µl of 1/3 strength liquid KB per well at 20 °C with agitation for 72 h. Cell-free supernatants were obtained by filter sterilization (0.22 µm) using Multiscreen HTS 96-well filtration plates (1000 × g, 30 min), which were used to measure the production of the plant hormone auxin (Indole-3-acetic acid (IAA)), iron-chelating siderophores and proteolytic activity. Furthermore, we also measured antifungal and antibacterial activity of all colonies.

IAA detection: The production of the plant hormone auxin was determined with a colorimetric test [49]. Briefly, 30 µl *P. protegens* CHA0 cell-free filtrate was incubated with 30 µl R1 reagent (12 g l^{-1} $FeCl_3$, 7.9 M H_2SO_4) for 12 h in the dark and optical density read at 530 nm of the colorimetric complex was used as a measurement of IAA concentration.

Siderophore activity: Iron chelating ability was measured as a proxy for siderophore production [50]. To this end, 100 µl of *P. protegens* CHA0 cell-free filtrate was mixed with 100 µl of modified CAS solution (with 0.15 mM $FeCl_3$) and optical density read at 630 nm after 3 hours of incubation was used as a proxy of siderophore production. The iron chelating ability was calculated based on the standard curve based on modified CAS assay solution with a range of iron concentration (0, 0.0015, 0.003, 0.006, 0.009, 0.012, 0.015 mM $FeCl_3$).

Proteolytic activity: The proteolytic activity assay we used was adapted from Smeltzer et al. (1993) [51]. Briefly, 15 µl of *P. protegens* CHA0 cell-free filtrate was incubated with 25 µl of

bioRxiv preprint doi: https://doi.org/10.1101/2020.12.07.414607; this version posted December 7, 2020. The copyright holder for this preprint (which was not certified by peer review) is the author/funder, who has granted bioRxiv a license to display the preprint in perpetuity. It is made available under aCC-BY 4.0 International license.

483 azocasein (2% w/v in 50 mM Tris-HCl pH 8.0) at 40 °C for 24 hours. 125 µl of 10% w/v cold
484 trichloroacetic acid (TCA) was added to precipitate superfluous azocasein, and then 100 µl
485 supernatant was neutralized with 100 µl of 1M NaOH after centrifugation at 5000 rpm for 30
486 minutes. Optical density read at 440 nm was used as a proxy of exoprotease activity.

487 **Tryptophan side chain oxidase (TSO) activity:** TSO activity, an indicator of quorum sensing
488 activity in *P. protegens* CHA0, was measured based on an modified established colorimetric assay
489 [52]: Three-day-old bacterial cultures grown in 1/3 strength liquid KB were mixed at a 1:1 ratio with
490 a reagent solution (5 g l^{-1} SDS, 37.6 g l^{-1} glycine 2.04 l^{-1} g tryptophan, pH 3.0) and TSO activity
491 was measured as optical density at 600 nm after overnight incubation.

492 **Biofilm formation:** We quantified bacterial biofilm formation using a standard protocol [53]. Briefly,
493 bacteria were grown at 20 °C for 72h in 160 µl 1 g l^{-1} TSB in 96-well microtiter plate with TSP lid
494 (TSP, NUNC, Roskilde, Denmark). Planktonic cells were removed by immersing the lid with pegs
495 three times in phosphate-buffered saline solution (PBS). Subsequently, the biofilm on the pegs was
496 stained for 20 minutes in 160 µl 1% Crystal Violet solution. Pegs were washed five times in PBS
497 after which the Crystal Violet was extracted for 20 minutes from the biofilm in a new 96-well
498 microtiter plate containing 200 µl 96% ethanol per well. Biofilm formation was defined as the
499 optical density at 590 nm of the ethanol extracted Chrystal Violet [54].

500 **Inhibition of other microorganisms:** Antimicrobial activity was defined as the relative growth of
501 the target organism in *P. protegens* supernatant compared to the control treatment. Antifungal
502 activity of the cell-free supernatant was assessed against the ascomycete *Verticillium dahlia*. The
503 fungus was grown on potato dextrose agar (PDA) at 28 °C for 4 days, after which plugs of fungal
504 mycelium were incubated in potato dextrose broth (PDB) medium at 28 °C and gentle shaking for
505 5 days. Fungal spores were collected by filtering out the mycelium from this culture over glass

bioRxiv preprint doi: https://doi.org/10.1101/2020.12.07.414607; this version posted December 7, 2020. The copyright holder for this preprint (which was not certified by peer review) is the author/funder, who has granted bioRxiv a license to display the preprint in perpetuity. It is made available under aCC-BY 4.0 International license.

wool. Subsequently, spores were washed and resuspended in water and the OD_{595} of the suspension was adjusted to 1. Five µl of this spore suspension was then inoculated with 15 µl *P. protegens* CHA0 cell-free filtrate and incubated in 160 µl of 1g l^{-1} PDB medium for 2 days at 20 °C in 96 well plates. Fungal growth was measured as optical density at 595 nm after 2 days of growth and contrasted with the growth in the control treatment (PDB medium without *P. protegens* supernatant). Antibacterial activity was determined using the plant pathogen *Ralstonia solanacearum* as a target organism. *R. solanacearum* was grown in 160 µl of 1 g l^{-1} TSB medium supplemented with 15 µl of *P. protegens* CHA0 cell-free filtrate or 15 µl of 1/3 strength liquid KB as a control for 2 days at 20 °C. *R. solanacearum* growth was measured as optical density at 600 nm.

Determining changes in *P. protegens* CHA0 interactions with *A. thaliana* after the selection experiment

Based on the life-history trait measurements, five distinct bacterial phenotypes were identified using K-means clustering analysis (Fig S2). In order to assess whether phenotypic changes reflected shifts in the strength and type of plant-bacterium interaction, we chose five isolates from each bacterial phenotype group representing each replicate selection line and five ancestral isolates for further measurements (a total of 30 isolates, Table S2).

a. *Effects of ancestor and evolved bacteria on plant performance*

For each isolate we measured root colonizing ability and impact on plant performance. All 30 bacterial isolates were incubated overnight in 1/3 KB strength liquid at 20 °C. The culture was centrifuged twice for five minutes at 5000 x g and the pellet was washed and finally resuspended

bioRxiv preprint doi: https://doi.org/10.1101/2020.12.07.414607; this version posted December 7, 2020. The copyright holder for this preprint (which was not certified by peer review) is the author/funder, who has granted bioRxiv a license to display the preprint in perpetuity. It is made available under aCC-BY 4.0 International license.

in 10 mM $MgSO_4$. The resulting suspension was adjusted to an OD_{600} of 0.01 for each strain as described previously [55]. Ten µl of the bacterial suspension (or 10 mM $MgSO_4$ as a control) was applied to the roots of three 10-day old sterile *Arabidopsis thaliana* Col-0 seedlings (excluding 2-days of stratification at 4 °C) grown on vertically positioned Petri dishes with agar-solidified (1.5% agar (w/v)) modified Hoagland's medium (n = 3 biological plant replicates, each containing 3 seedlings). Plants were grown for 14 days before harvesting. Plants were photographed before and 14 days after bacterial inoculation.

Bacterial effects on plant health were quantified as leaf 'greenness' as the presence of ancestral strain was observed to lead to bleaching and loss of chlorophyll in *A. thaliana* leaves. The 'greenness' was quantified from photographs by measuring the number of green pixels. To this end, photographs were first transformed in batch using Adobe Photoshop 2021 by sequentially selecting only green areas followed by thresholding balancing green tissue over background noise (Level 80). This resulted in black-and-white images for further analysis, and the mean number of white pixels per fixed-sized region-of-interest of the aboveground tissue was subsequently determined as 'greenness' using ImageJ. The numbers of lateral roots and the primary root length were also measured using ImageJ (version 1.50i). The root morphology data measured at the end of the experiment was normalized with the data collected at the time of inoculation for each individual seedling.

To determine shoot biomass, the rosette of each plant was separated from the root system with a razor blade and weighted. The roots were placed into a pre-weighted 1.5 ml Eppendorf tubes to quantify the root biomass. Then these tubes were filled with 1 ml 10 mM $MgSO_4$ buffer solution and two glass beads. The rhizosphere bacteria were suspended into buffer solution using TissueLyser II at a frequency of 20 s^{-1} for 1 min after which bacterial densities were determined using flow cytometry as described above.

bioRxiv preprint doi: https://doi.org/10.1101/2020.12.07.414607; this version posted December 7, 2020. The copyright holder for this preprint (which was not certified by peer review) is the author/funder, who has granted bioRxiv a license to display the preprint in perpetuity. It is made available under aCC-BY 4.0 International license.

553 Shoot biomass, root biomass, root length, and number of lateral roots were used in a
554 principal component analysis (PCA) to calculate an overall impact of the bacteria on plant
555 performance (Fig 2E). The first principal component (PC1) explained 79.9% of the variation and
556 was normalized against the control treatment to be used as a proxy of 'Plant performance' in which
557 positive values reflect plant growth promotion and negative values plant growth inhibition.

558 ***b. Root derived carbon source utilization***

559 To measure changes in bacterial growth on potential root derived carbon sources, we measured the
560 growth of all 256 isolates using modified Ornston and Stanier (OS) minimal medium [56]
561 supplemented with single carbon sources at a final concentration of 0.5g l^{-1} in 96-well plates
562 containing 160 µl carbon supplemented OS medium per well. The following carbon sources were
563 selected based on their relatively high abundance in *Arabidopsis* root exudates[21]: alanine,
564 arabinose, butyrolactam, fructose, galactose, glucose, glycerol, glycine, lactic acid, putrescine,
565 serine, succinic acid, threonine and valine. Bacterial growth was determined by measuring optical
566 density at 600 nm after three days incubation at 20 °C.

567 ***c.* GUS *histochemical staining assay and bacterial growth under scopoletin stress***

568 To investigate effects of the ancestor and evolved strains of *P. protegens* CHA0 on expression of
569 *MYB72* gene, we applied *GUS* histochemical staining assay to the 30 selected isolates (Table S2).
570 MYB72 is a transcription factor involved in production of the coumarin scopoletin in *Arabidopsis*
571 roots and specific rhizobacteria can upregulate expression of *MYB72* in the roots. Scopoletin is an
572 iron-mobilizing phenolic compound with selective antimicrobial activity [22]. Seedlings of the *A.*
573 *thaliana* $MYB72_{pro}$*:GFP-GUS* [24] reporter line were prepared as described above. Seven day old
574 seedlings were inoculated directly below the hypocotyls with 10 µl of a bacterial suspension
575 (OD660 = 0.1) as described previously [24]. At 2 days after inoculation, the roots were separated

bioRxiv preprint doi: https://doi.org/10.1101/2020.12.07.414607; this version posted December 7, 2020. The copyright holder for this preprint (which was not certified by peer review) is the author/funder, who has granted bioRxiv a license to display the preprint in perpetuity. It is made available under aCC-BY 4.0 International license.

576 from the shoots and washed in Milli-Q water (Milliport Corp., Bedford, MA) to remove all the
577 adhered bacteria. GUS staining of the roots was performed in 12-well microtiter plates where each
578 well contained roots of 5 to 6 seedlings and 1 mL of freshly prepared GUS substrate solution (50
579 mM sodium phosphate with a pH at 7, 10 mM EDTA, 0.5 mM K4[Fe(CN)6], 0.5 mM
580 K3[Fe(CN)6], 0.5 mM X-Gluc, and 0.01% Silwet L-77) as described previously [57]. Plates were
581 incubated in the dark at room temperature for 16 h. The roots were fixed overnight in 1mL
582 ethanol:acetic acid (3:1 v/v) solution at 4 ℃ and transferred to 75% ethanol. Then the pictures of
583 each microtiter plates were taken, and GUS activity was quantified by counting the number of blue
584 pixels in each well of the microtiter plates using image analysis in ImageJ (version 1.52t). To assess
585 the effects of scopoletin on ancestral and evolved *P. protegens* CHA0 isolates, we applied a
586 sensitivity assay to the 30 selected isolates (Table S2). In brief, growth of bacterial isolates was
587 measured in 1 g l^{-1} TSB medium (160 µl) supplemented with scopoletin at final concentrations of
588 0 µM (control), 500 µM, 1000 µM, and 2 mM using optical density at 600 nm after 96 h incubation
589 at 20 °C without shaking in 96-well microtiter plates. Maximal effect (Emax) of scopoletin was
590 calculated via R package 'GRmetrics' [58] as an indication of scopoletin tolerance.
591

592 **Whole genome sequencing**

593 All 30 isolated phenotypes were whole genome sequenced to identify possible mutations and
594 affected genes. To this end, isolates were cultured overnight at 28 °C in 1/3 strength liquid KB.
595 Chromosomal DNA was isolated from each culture using the GenElute™ Bacterial Genomic DNA
596 Kit Protocol (NA2100). DNA samples were sheared on a Covaris E-220 Focused-ultrasonicator
597 and sheared DNA was then used to prepare Illumina sequencing libraries with the NEBNext®
598 Ultra™ DNA Library Prep Kit (New England Biolabs. France) and the NEBNext® Multiplex

bioRxiv preprint doi: https://doi.org/10.1101/2020.12.07.414607; this version posted December 7, 2020. The copyright holder for this preprint (which was not certified by peer review) is the author/funder, who has granted bioRxiv a license to display the preprint in perpetuity. It is made available under aCC-BY 4.0 International license.

599 Oligos for Illumina® (96 Index Primers). The final libraries were sequenced in multiplex on the
600 NextSeq 500 platform (2 x 75 bp paired-end) by the Utrecht Sequencing Facility
601 (http://www.useq.nl) yielding between 1.0 and 6.4 million reads per sample equivalent to ~10 – 70
602 fold coverage (based on comparison with the original 6.8 Mbp reference genome NCBI GenBank:
603 CP003190.1).
604

605 ## Variant calling analysis

606 We first constructed an updated reference genome of *P. protegens* CHA0, carrying the *GFP* marker
607 gene on its chromosome, from the ancestral strain using the A5 pipeline with default parameters
608 [59]. The input dataset for this sample consisted of 3,1 M reads and totals an approximate 34-fold
609 coverage. The size of the updated reference genome is 6.8 Mbp, with a G+C content of 63.4%, and
610 it comprises 80 scaffolds, with a N_{50} value of 343 Kbp. We subsequently used PROKKA [60] (version
611 1.12; https://github.com/tseemann/prokka) for full annotation of the updated reference genome,
612 and this resulted in the identification of 6,147 genes. The updated genome is deposited in NCBI
613 GenBank with following reference: RCSR00000000.1.

614 Having established the ancestral genome sequence, we subsequently used Snippy (version
615 3.2-dev; https://github.com/tseemann/snippy) to identify and functionally annotate single
616 nucleotide polymorphisms and small insertions and deletions (indels) for each individual strain. In
617 addition, we investigated the breadth of coverage for each gene per sample with BedTools [61] to
618 identify genes with large insertions or deletions. An overview of the polymorphisms is shown in
619 Supplementary Table S3. Raw sequencing data for this study is deposited at the NCBI database
620 under BioProject PRJNA473919.
621

bioRxiv preprint doi: https://doi.org/10.1101/2020.12.07.414607; this version posted December 7, 2020. The copyright holder for this preprint (which was not certified by peer review) is the author/funder, who has granted bioRxiv a license to display the preprint in perpetuity. It is made available under aCC-BY 4.0 International license.

Relative competitive fitness of *gac* mutants measured *in vivo* and *in vitro*

The relative competitive fitness of selected *gac* mutants was measured in direct competition with their direct ancestors both *in vivo* in the rhizosphere of *A. thaliana* and *in vitro* in different standard culture media. Relative fitness was measured as deviation from initial 1:1 ratio of bacterial clone pairs based on PCR-based high-resolution melting profile (RQ-HRM) analysis. Three pairs of isolates were selected: A) Evolved *gacA* ID 242 (genotype $oafA^{Y335X}$ · $RS17350^{A77A.fsX14}$ · $gacA^{D49Y}$) and its direct ancestral genotype 133 (genotype $oafA^{Y335X}$ · $RS17350^{A77A.fsX14}$) from evolutionary line 1; B) Evolved *gacA* ID 220 (genotype $galE^{V32M}$ · $accC^{E413K}$ · $gacA^{D54Y}$) and its direct ancestral genotype 28 (genotype $galE^{V32M}$ · $accC^{E413K}$) from line 2; C) Evolved *gacS* ID 222 (genotype $oafA^{K338S.fsX18}$ · $gacS^{G27D}$) and its direct ancestral genotype 66 (genotype $oafA^{K338S.fsX18}$) from line 3. Bacterial isolates were first grown overnight in KB medium at 28 °C, centrifuged at 4,500 rpm for 10 min and the pellet resuspended in 10 mM $MgSO_4$. This washing procedure was repeated twice. The resulting bacterial suspensions were diluted to OD_{600} = 0.05. The initial inoculum for the competition assays was then generated by mixing equal volumes of evolved and ancestral competitors in a ratio of 1:1.

Measuring competitive fitness in A. thaliana rhizosphere

This assay was performed on the roots of 10-day old *A. thaliana* seedlings grown on full strength Hoagland agar plates, which were prepared as described earlier. Twenty µl of the initial inoculum, containing a total of 10^6 bacterial cells, was inoculated on to the root-shoot junction of each seedling. After 14 days of growth, bacterial populations were isolated from the roots as described earlier and stored at -80 °C in 42.5% glycerol for relative abundance measurements.

bioRxiv preprint doi: https://doi.org/10.1101/2020.12.07.414607; this version posted December 7, 2020. The copyright holder for this preprint (which was not certified by peer review) is the author/funder, who has granted bioRxiv a license to display the preprint in perpetuity. It is made available under aCC-BY 4.0 International license.

Measuring competitive fitness in culture media

Competition assays were also performed in three commonly used nutrient-rich growth media: Kings' B (KB), lysogeny broth (LB), and tryptic soy broth (TSB). KB contained 20 g proteose peptone, 1.5 g $MgSO_4.7H_2O$, 1.2 g KH_2PO_4 and 10 g glycerol per litre and the pH was adjusted to 7.3 ± 0.2. TSB contained 30 g tryptic soy broth per litre and pH was adjusted to 7.3 ± 0.2. LB contained 10 g peptone, 5 g yeast extract and 5 g NaCl per litre. Twenty µl inoculum of competing strains, containing about 10^6 bacterial cells, were added into wells containing 140 µl fresh medium in a 96-well plate. The microplates were incubated at 28 °C without shaking for 48 after 80 µl sample was harvested and stored at -80 °C in 42.5% glycerol from each well for relative abundance measurements.

RQ-HRM assay for quantifying changes in genotype frequencies after competition

We used a High-Resolution Melting (HRM) curve profile assay with integrated LunaProbes to quantify the ratio of mutant to wild type genotypes [62–64]. The probes and primers used in this study are listed in Table S4. Primers were designed using Primer3. Probes were designed with the single nucleotide polymorphism (SNP) located in the middle of the sequence, and the 3' end was blocked by carbon spacer C3. The primer asymmetry was set to 2:1 (excess primer: limiting primer) in all cases. Pre-PCR was performed in a 10-µl reaction system, with 0.25 µM excess primer, 0.125 µM limiting primer, 0.25 µM probe, 0.5 µl bacterial sample culture (100-fold diluted saved sample, OD_{600} is about 0.01), 1X LightScanner Master Mix (BioFire Defense). DMSO with the final concentration 5% was supplemented in all reactions to ensure the targeted melting domains are within the detection limit of the LightScanner (Idaho Technology Inc.). Finally, MQ water was used to supplement up to 10 µl. A 96-well black microtiter plate with white wells was used to

bioRxiv preprint doi: https://doi.org/10.1101/2020.12.07.414607; this version posted December 7, 2020. The copyright holder for this preprint (which was not certified by peer review) is the author/funder, who has granted bioRxiv a license to display the preprint in perpetuity. It is made available under aCC-BY 4.0 International license.

minimize background fluorescence. Before amplification, 25 µl mineral oil was loaded in each well to prevent evaporation, and the plate was covered with a foil seal to prevent the degradation of fluorescent molecules. Amplification was initiated by a holding at 95 °C for 3 min, followed by 55 cycles of denaturation at 95 °C for 30 s, annealing at 60 °C for 30 s and extension at 72 °C for 30 s and then kept at 72 °C for 10 min. After amplification, samples were heated in a ThermalCycler (Bio-Rad) shortly to 95 °C for 30 s to denature all double-stranded structures followed by a rapid cooling to 25 °C for 30 s to facilitate successful hybridization between probes and the target strands. The plate was then transferred to a LightScanner (Idaho Technology Inc.). Melting profiles of each well were collected by monitoring the continuous loss of fluorescence with a steady increase of the temperature from 35 °C to 97 °C with a ramp rate of 0.1 °C /s. The relative quantification was based on the negative first derivative plots using software MATLAB. The areas of probe-target duplexes melting peaks were auto-calculated by 'AutoFit Peaks I Residuals' function in software PeakFit (SeaSolve Software Inc.). The mutant frequency X was calculated using the formula shown below:

$$X = \frac{\text{Area}_{mutant}}{\text{Area}_{mutant} + \text{Area}_{WT}}$$

To validate the RQ-HRM method, standard curves were generated by measuring mixed samples with known proportions of mutant templates: 0%, 10%, 20%, 30%, 40%, 50%, 60%, 70%, 80%, 90% and 100%. Measurements for each sample were done in triplicate. Linear regression formula of each mutant between actual frequencies and measured frequencies were shown in Figure S7. The high R^2 values, and nearly equal to 1 slope values of these equations, confirmed that the RQ-HRM method can accurately detect mutants' frequency in a mixed population.

bioRxiv preprint doi: https://doi.org/10.1101/2020.12.07.414607; this version posted December 7, 2020. The copyright holder for this preprint (which was not certified by peer review) is the author/funder, who has granted bioRxiv a license to display the preprint in perpetuity. It is made available under aCC-BY 4.0 International license.

689 The relative fitness of the evolved strains was calculated according to previous studies using the

690 following equation [65,66]:

691 $$\text{Relative fitness (r)} = \frac{X_1(1 - X_0)}{X_0(1 - X_1)}$$

692 X_0: initial mutant frequency; (1-X_0): initial ancestor frequency. X_1: final mutant frequency; (1-X_1):

693 final ancestor frequency.

694

bioRxiv preprint doi: https://doi.org/10.1101/2020.12.07.414607; this version posted December 7, 2020. The copyright holder for this preprint (which was not certified by peer review) is the author/funder, who has granted bioRxiv a license to display the preprint in perpetuity. It is made available under aCC-BY 4.0 International license.

695 **References and Notes:**

696 1. Berendsen, R. L., Pieterse, C. M. J. & Bakker, P. A. H. M. The rhizosphere microbiome
697 and plant health. *Trends Plant Sci.* **17**, 478–486 (2012).
698 2. Philippot, L., Raaijmakers, J. M., Lemanceau, P. & van der Putten, W. H. Going back to
699 the roots: the microbial ecology of the rhizosphere. *Nat. Rev. Microbiol.* **11**, 789–799
700 (2013).
701 3. Dethlefsen, L., McFall-Ngai, M. & Relman, D. A. An ecological and evolutionary
702 perspective on human–microbe mutualism and disease. *Nature* **449**, 811–818 (2007).
703 4. Brownlie, J. C. & Johnson, K. N. Symbiont-mediated protection in insect hosts. *Trends*
704 *Microbiol.* **17**, 348–354 (2009).
705 5. Kiers, E. T. & Denison, R. F. Sanctions, cooperation, and the stability of plant-rhizosphere
706 mutualisms. *Annu. Rev. Ecol. Evol. Syst* **39**, 215–236 (2008).
707 6. King, K. C. *et al.* Rapid evolution of microbe-mediated protection against pathogens in a
708 worm host. *ISME J.* **10**, 1915–1924 (2016).
709 7. Tso, G. H. W. *et al.* Experimental evolution of a fungal pathogen into a gut symbiont.
710 *Science* **362**, 589–595 (2018).
711 8. Berendsen, R. L. *et al.* Disease-induced assemblage of a plant-beneficial bacterial
712 consortium. *ISME J.* **12**, 1496–1507 (2018).
713 9. Sasse, J., Martinoia, E. & Northen, T. Feed your friends: do plant exudates shape the root
714 microbiome? *Trends Plant Sci.* **23**, 25–41 (2018).
715 10. Bakker, P. A. H. M., Pieterse, C. M. J., de Jonge, R. & Berendsen, R. L. The soil-borne
716 legacy. *Cell* **172**, 1178–1180 (2018).
717 11. Johnson, N. C., Graham, J. H. & Smith, F. A. Functioning of mycorrhizal associations
718 along the mutualism-parasitism continuum. *New Phytol.* **135**, 575–586 (1997).
719 12. Kogel, K. H., Franken, P. & Hückelhoven, R. Endophyte or parasite - what decides? *Curr.*
720 *Opin. Plant Biol.* **9**, 358–363 (2006).
721 13. Cosme, M., Fernández, I., Van der Heijden, M. G. A. & Pieterse, C. M. J. Non-
722 mycorrhizal plants: the exceptions that prove the rule. *Trends in Plant Science* **23**, 577–
723 587 (2018).
724 14. Wein, T. *et al.* Currency, exchange, and inheritance in the evolution of symbiosis. *Trends*
725 *Microbiol.* **27**, 836–849 (2019).
726 15. Chomicki, G., Kiers, E. T. & Renner, S. S. The evolution of mutualistic dependence. *Annu.*
727 *Rev. Ecol. Evol. Syst.* **51**, annurev-ecolsys-110218-024629 (2020).
728 16. Stringlis, I. A., Zhang, H., Pieterse, C. M. J., Bolton, M. D. & De Jonge, R. Microbial
729 small molecules-weapons of plant subversion. *Natural Product Reports* **35**, 410–433
730 (2018).
731 17. Kramer, J., Özkaya, Ö. & Kümmerli, R. Bacterial siderophores in community and host
732 interactions. *Nature Reviews Microbiology* **18**, 152–163 (2020).
733 18. Kawecki, T. J. *et al.* Experimental evolution. *Trends Ecol. Evol.* **27**, 547–560 (2012).
734 19. Jousset, A., Lara, E., Wall, L. G. & Valverde, C. Secondary metabolites help biocontrol
735 strain *Pseudomonas fluorescens* CHA0 to escape protozoan grazing. *Appl. Environ.*
736 *Microbiol.* **72**, 7083–7090 (2006).
737 20. Brazelton, J. N., Pfeufer, E. E., Sweat, T. A., Gardener, B. B. M. & Coenen, C. 2 , 4-
738 Diacetylphloroglucinol alters plant root development. *Mol. Plant-Microbe Interact.* **21**,
739 1349–1358 (2008).
740 21. Chaparro, J. M. *et al.* Root exudation of phytochemicals in *Arabidopsis* follows specific
741 patterns that are developmentally programmed and correlate with soil microbial functions.

bioRxiv preprint doi: https://doi.org/10.1101/2020.12.07.414607; this version posted December 7, 2020. The copyright holder for this preprint (which was not certified by peer review) is the author/funder, who has granted bioRxiv a license to display the preprint in perpetuity. It is made available under aCC-BY 4.0 International license.

PLoS One **8**, e55731 (2013).
22. Stringlis, I. A. *et al.* MYB72-dependent coumarin exudation shapes root microbiome assembly to promote plant health. *Proc. Natl. Acad. Sci. U. S. A.* **115**, E5213–E5222 (2018).
23. Voges, M. J. E. E. E., Bai, Y., Schulze-Lefert, P. & Sattely, E. S. Plant-derived coumarins shape the composition of an *Arabidopsis* synthetic root microbiome. *Proc. Natl. Acad. Sci. U. S. A.* **116**, 12558–12565 (2019).
24. Zamioudis, C. *et al.* Rhizobacterial volatiles and photosynthesis-related signals coordinate *MYB72* expression in Arabidopsis roots during onset of induced systemic resistance and iron-deficiency responses. *Plant J.* **84**, 309–322 (2015).
25. Barrick, J. E. & Lenski, R. E. Genome dynamics during experimental evolution. *Nat. Rev. Genet.* **14**, 827–839 (2013).
26. Yang, L. *et al.* Evolutionary dynamics of bacteria in a human host environment. *Proc. Natl. Acad. Sci.* **108**, 7481–7486 (2011).
27. Haas, D. & Défago, G. Biological control of soil-borne pathogens by fluorescent pseudomonads. *Nat. Rev. Microbiol.* **3**, 307–319 (2005).
28. Reyrat, J. M., David, M., Batut, J. & Boistard, P. FixL of *Rhizobium meliloti* enhances the transcriptional activity of a mutant FixJD54N protein by phosphorylation of an alternate residue. *J. Bacteriol.* **176**, 1969–1976 (1994).
29. Laville, J. *et al.* Global control in *Pseudomonas fluorescens* mediating antibiotic synthesis and suppression of black root rot of tobacco. *Proc. Natl. Acad. Sci.* **89**, 1562–1566 (1992).
30. Bull, C. T. *et al.* Characterization of spontaneous *gacS* and *gacA* regulatory mutants of *Pseudomonas fluorescens* biocontrol strain CHA0. *Antonie Van Leeuwenhoek* **79**, 327–336 (2001).
31. Zhang, R. *et al.* Structure of a bacterial quorum-sensing transcription factor complexed with pheromone and DNA. *Nature* **417**, 971–974 (2002).
32. Battesti, A., Majdalani, N. & Gottesman, S. The RpoS-mediated general stress response in *Escherichia coli*. *Annu. Rev. Microbiol* **65**, 189–213 (2011).
33. Stockwell, V. O. & Loper, J. E. The sigma factor RpoS is required for stress tolerance and environmental fitness of *Pseudomonas fluorescens* Pf-5. *Microbiology* **151**, 3001–3009 (2005).
34. Heeb, S., Valverde, C. & Haas, D. Role of the stress sigma factor RpoS in GacA / RsmA-controlled secondary metabolism and resistance to oxidative stress in *Pseudomonas fluorescens* CHA0. *FEMS Microbiol. Lett.* **243**, 251–258 (2005).
35. Whiteley, M. *et al.* Gene expression in *Pseudomonas aeruginosa* biofilms. *Nature* **413**, 860–864 (2001).
36. Ramey, B. E., Koutsoudis, M., Bodman, S. B. V. & Fuqua, C. Biofilm formation in plant-microbe associations. *Current Opinion in Microbiology* **7**, 602–609 (2004).
37. Fukami, T., Beaumont, H. J. E., Zhang, X. X. & Rainey, P. B. Immigration history controls diversification in experimental adaptive radiation. *Nature* **446**, 436–439 (2007).
38. Fukami, T. Historical contingency in community assembly: integrating niches, species pools, and priority effects. *Annu. Rev. Ecol. Evol. Syst.* **46**, 1–23 (2015).
39. Rainey, P. B. & Travisano, M. Adaptive radiation in a heterogeneous environment. *Nature* **394**, 69–70 (1998).
40. Gómez, P. & Buckling, A. Real-time microbial adaptive diversification in soil. *Ecol. Lett.* **16**, 650–655 (2013).
41. Houte, S. *et al.* Compost spatial heterogeneity promotes evolutionary diversification of a

bioRxiv preprint doi: https://doi.org/10.1101/2020.12.07.414607; this version posted December 7, 2020. The copyright holder for this preprint (which was not certified by peer review) is the author/funder, who has granted bioRxiv a license to display the preprint in perpetuity. It is made available under aCC-BY 4.0 International license.

789 bacterium. *J. Evol. Biol.* jeb.13722 (2020). doi:10.1111/jeb.13722
790 42. Klironomos, J. N. Feedback with soil biota contributes to plant rarity and invasiveness in
791 communities. *Nature* **417**, 67–70 (2002).
792 43. Kardol, P., Martijn Bezemer, T. & van der Putten, W. H. Temporal variation in plant-soil
793 feedback controls succession. *Ecol. Lett.* **9**, 1080–1088 (2006).
794 44. Batstone, R. T., O'Brien, A. M., Harrison, T. L. & Frederickson, M. E. Experimental
795 evolution makes microbes more cooperative with their local host genotype. *Science* **370**,
796 476–478 (2020).
797 45. Ramette, A. *et al. Pseudomonas protegens* sp. nov., widespread plant-protecting bacteria
798 producing the biocontrol compounds 2,4-diacetylphloroglucinol and pyoluteorin. *Syst.*
799 *Appl. Microbiol.* **34**, 180–188 (2011).
800 46. Stutz, E. W., Défago, G. & Kern, H. Naturally occurring fluorescent pseudomonads
801 involved in suppression of black root rot of tobacco. *Phytopathology* **76**, 181–185 (1986).
802 47. Jousset, A. *et al.* Full-genome sequence of the plant growth-promoting bacterium
803 *Pseudomonas protegens* CHA0. *Genome Announc.* **2**, e00322-14 (2014).
804 48. King, E. O., Ward, M. K. & Raney, D. E. Two simple media for the demonstration of
805 pyocyanin and fluorescin. *J. Lab. Clin. Med.* **44**, 301–307 (1954).
806 49. Glickmann, E. & Dessaux, Y. A critical examination of the specificity of the salkowski
807 reagent for indolic compounds produced by phytopathogenic bacteria. *Appl. Environ.*
808 *Microbiol.* **61**, 793–796 (1995).
809 50. Alexander, D. B. & Zuberer, D. A. Use of chrome azurol S reagents to evaluate
810 siderophore production by rhizosphere bacteria. *Biol. Fertil. Soils* **12**, 39–45 (1991).
811 51. Smeltzer, M. S., Hart, M. E. & Iandolo, J. J. Phenotypic characterization of *xpr*, a global
812 regulator of extracellular virulence factors in *Staphylococcus aureus*. *Infect. Immun.* **61**,
813 919–925 (1993).
814 52. Oberhänsli, T., Défago, G. & Haas, D. Indole-3-acetic acid (IAA) synthesis in the
815 biocontrol strain CHA0 of *Pseudomonas fluorescens*: role of tryptophan side chain
816 oxidase. *Microbiology* **137**, 2273–2279 (1991).
817 53. Moskowitz, S. M., Foster, J. M., Emerson, J. & Burns, J. L. Clinically feasible biofilm
818 susceptibility assay for isolates of *Pseudomonas aeruginosa* from patients with cystic
819 fibrosis. *J. Clin. Microbiol.* **42**, 1915–1922 (2004).
820 54. Harrison, J. J. *et al.* Microtiter susceptibility testing of microbes growing on peg lids: a
821 miniaturized biofilm model for high-throughput screening. *Nat. Protoc.* **5**, 1236–1254
822 (2010).
823 55. Zamioudis, C., Mastranesti, P., Dhonukshe, P., Blilou, I. & Pieterse, C. M. J. Unraveling
824 root developmental programs initiated by beneficial *Pseudomonas* spp bacteria. *Plant*
825 *Physiol.* **162**, 304–318 (2013).
826 56. Højberg, O., Schnider, U., Winteler, H. V, Sørensen, J. & Haas, D. Oxygen-sensing
827 reporter strain of *Pseudomonas fluorescens* for monitoring the distribution of low-oxygen
828 habitats in soil. *Appl. Environ. Microbiol.* **65**, 4085–4093 (1999).
829 57. Millet, Y. A. *et al.* Innate immune responses activated in *Arabidopsis* roots by microbe-
830 associated molecular patterns. *Plant Cell* **22**, 973–990 (2010).
831 58. Hafner, M., Niepel, M., Chung, M. & Sorger, P. K. Growth rate inhibition metrics correct
832 for confounders in measuring sensitivity to cancer drugs. *Nat. Methods* **13**, 521–527
833 (2016).
834 59. Tritt, A., Eisen, J. A., Facciotti, M. T. & Darling, A. E. An integrated pipeline for de novo
835 assembly of microbial genomes. *PLoS One* **7**, e42304 (2012).

bioRxiv preprint doi: https://doi.org/10.1101/2020.12.07.414607; this version posted December 7, 2020. The copyright holder for this preprint (which was not certified by peer review) is the author/funder, who has granted bioRxiv a license to display the preprint in perpetuity. It is made available under aCC-BY 4.0 International license.

836 60. Seemann, T. Prokka: rapid prokaryotic genome annotation. *Bioinformatics* **30**, 2068–2069
837 (2014).
838 61. Quinlan, A. R. & Hall, I. M. BEDTools: a flexible suite of utilities for comparing genomic
839 features. *Bioinformatics* **26**, 841–842 (2010).
840 62. Kai Lee, H. *et al.* High-resolution melting approach to efficient identification and
841 quantification of H275Y mutant influenza H1N1/2009 virus in mixed-virus-population
842 samples. *J. Clin. Microbiol.* **49**, 3555–3559 (2011).
843 63. Zhong, W.-L. *et al.* Development of unlabeled probe based high-resolution melting
844 analysis for detection of filaggrin gene mutation c.3321delA. *J. Clin. Lab. Anal.* **30**, 892–
845 896 (2016).
846 64. Capper, R. L. *et al.* Quantitative high resolution melting: two methods to determine SNP
847 allele frequencies from pooled samples. *BMC Genet.* **16**, 62 (2015).
848 65. Jousset, A. *et al.* Predators promote defence of rhizosphere bacterial populations by
849 selective feeding on non-toxic cheaters. *ISME J.* **3**, 666–674 (2009).
850 66. Ross-Gillespie, A., Gardner, A., West, S. A. & Griffin, A. S. Frequency dependence and
851 cooperation: theory and a test with bacteria. *Am. Nat.* **170**, 331–342 (2007).
852

bioRxiv preprint doi: https://doi.org/10.1101/2020.12.07.414607; this version posted December 7, 2020. The copyright holder for this preprint (which was not certified by peer review) is the author/funder, who has granted bioRxiv a license to display the preprint in perpetuity. It is made available under aCC-BY 4.0 International license.

853 ## Acknowledgments:

854 We thank Roy van der Meijs for his excellent work on the scopoletin sensitivity assays and Ke Yu,
855 Roeland Berendsen and members of the Plant-Microbe Interactions lab for helpful discussion. This
856 work was supported by a China Scholarship Council fellowship (to E.L.), a postdoctoral fellowship
857 of the Research Foundation Flanders (FWO 12B8116RN) (to R.D.J.) and Royal Society Research
858 Grants (grant nos. RSG\R1\180213 and CHL\R1\180031) at the University of York (V-P.F).

859 ## Author contributions:

860 EL, PB and AJ designed the experiments. EL, HJ and CL performed the experiment. EL, RJ and
861 AJ analysed the data. All authors collegially wrote the manuscript.

862 ## Declaration of Interests:

863 Authors declare no competing interests**.**

864

bioRxiv preprint doi: https://doi.org/10.1101/2020.12.07.414607; this version posted December 7, 2020. The copyright holder for this preprint (which was not certified by peer review) is the author/funder, who has granted bioRxiv a license to display the preprint in perpetuity. It is made available under aCC-BY 4.0 International license.

Supplementary Materials for

Rapid evolution of bacterial mutualism in the plant rhizosphere

Data and materials availability:

The *P. protegens* CHA0-GFP reference strain genome sequence, determined for this study, is deposited on GenBank: RCSR00000000.1. Raw sequencing data used in this study are deposited at the NCBI database under BioProject PRJNA473919. Raw data of *P. protegens* CHA0 phenotypic traits, Supplementary dataset 1 and 2, are deposited at Mendeley Data: DOI: 10.17632/wh3ytm5rn8.1

The following file includes:

Figs. S1 to S7

Tables S1 to S4

Legends of supplementary dataset 1 and 2

bioRxiv preprint doi: https://doi.org/10.1101/2020.12.07.414607; this version posted December 7, 2020. The copyright holder for this preprint (which was not certified by peer review) is the author/funder, who has granted bioRxiv a license to display the preprint in perpetuity. It is made available under aCC-BY 4.0 International license.

878 **Supplementary figures:**

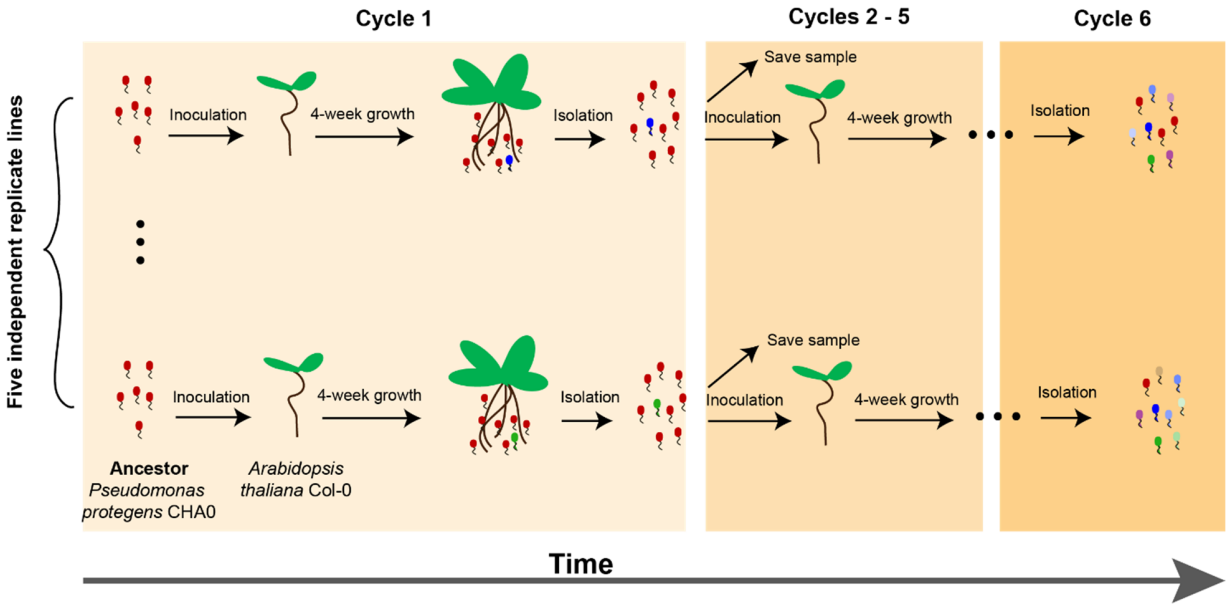

879

880 **Figure S1. Overview of the experimental design.** In this study, we experimentally evolved
881 *Pseudomonas protegens* CHA0 in the rhizosphere of sterile *Arabidopsis thaliana* plants**.** We used
882 a gnotobiotic, organic carbon-free soil system in which bacterial fitness strictly depended on their
883 interaction with plants. We set up five independent plant replicate lines, which were passed over
884 six plant growth cycles (4 weeks each). To this end, 10^6 cells of the ancestral *P. protegens* CHA0
885 strain were introduced to the rhizosphere of two *A. thaliana* seedlings grown in sterile silver sand
886 supplemented with a plant nutrient solution in sterile ECO2 boxes. At the end of each growth cycle,
887 the rhizosphere bacterial population was harvested, and 10^6 cells were inoculated onto a new plant.
888 The remaining bacteria were kept as frozen stock at -80 °C. At the end of the experiment, bacteria
889 from the -80 °C stock were plated on 3 g l^{-1} Tryptic Soy Agar and sixteen single bacterial isolates
890 were randomly selected from each replicate line at the end of the second, fourth and sixth growth
891 cycle. In total, 240 evolved isolates and sixteen ancestral isolates were phenotyped regarding traits
892 associated with bacterial fitness and mutualistic activity with the plant.

bioRxiv preprint doi: https://doi.org/10.1101/2020.12.07.414607; this version posted December 7, 2020. The copyright holder for this preprint (which was not certified by peer review) is the author/funder, who has granted bioRxiv a license to display the preprint in perpetuity. It is made available under aCC-BY 4.0 International license.

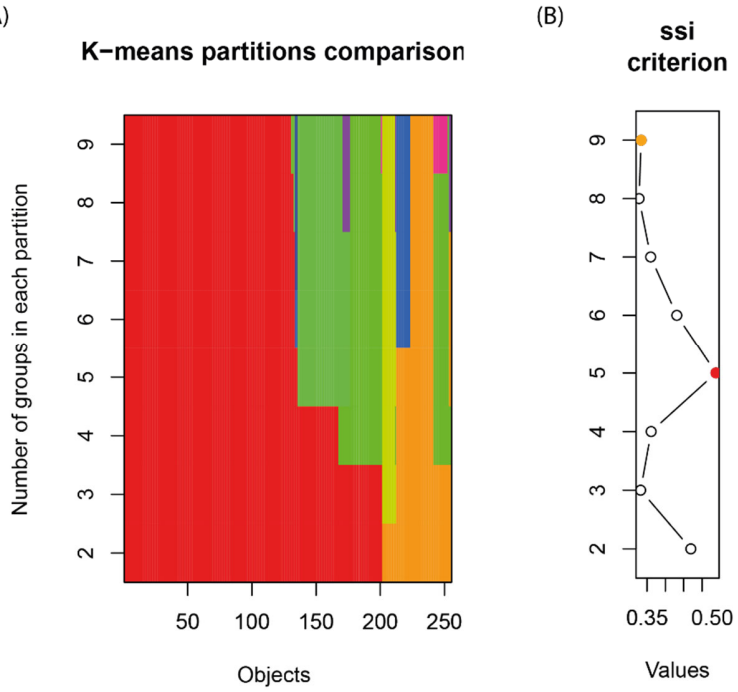

Figure S2. K-means clustering analysis of evolved *Pseudomonas protegens* CHA0 isolates. Isolated colonies were classified based on 14 phenotypic traits associated with bacterial fitness in the rhizosphere and mutualistic activity with the plant. In panel A, the x-axis ("Objects") represents the 256 screened isolates while the y-axis represents the potential number of clusters (K) shown in different colours. Panel B shows the SSI criterion values indicating the most parsimonious number of clusters needed to classify isolates into distinct phenotypic groups. Based on this analysis, we classified the isolates into five clusters (the highest SSI criterion value).

bioRxiv preprint doi: https://doi.org/10.1101/2020.12.07.414607; this version posted December 7, 2020. The copyright holder for this preprint (which was not certified by peer review) is the author/funder, who has granted bioRxiv a license to display the preprint in perpetuity. It is made available under aCC-BY 4.0 International license.

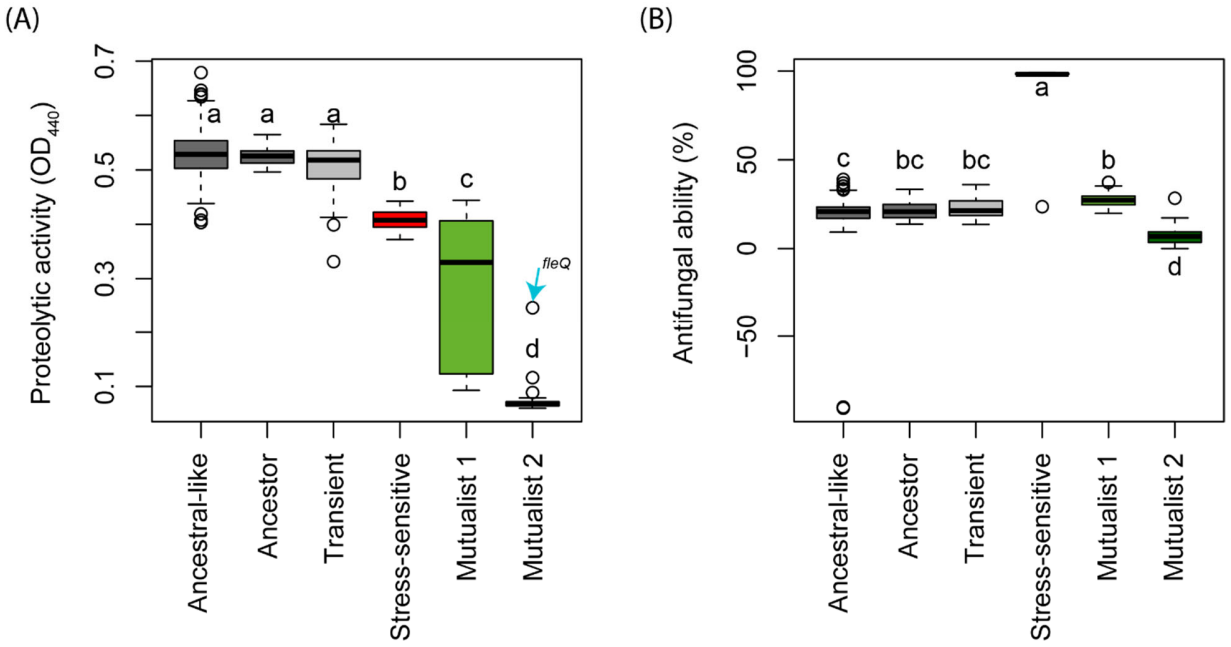

Figure S3. Comparing the differences in extracellular proteolytic and antifungal activity of ancestral and evolved *Pseudomonas protegens* CHA0 isolates. We measured the proteolytic (A) and antifungal activity (B) as a proxy for secondary metabolite production. In total, we characterized 16 ancestral, 119 ancestral-like, 11 stress-sensitive, 37 mutualist 1, 31 mutualist 2 and 41 transient isolates (Supplementary dataset 1). In panel A, the blue arrow indicates one isolate that was phenotypically clustered as mutualist 2, but genetically bearing a unique *fleQ* mutation. Statistical testing was carried out using ANOVA. Different letters indicate significant differences based on a Tukey HSD test (α=0.05).

bioRxiv preprint doi: https://doi.org/10.1101/2020.12.07.414607; this version posted December 7, 2020. The copyright holder for this preprint (which was not certified by peer review) is the author/funder, who has granted bioRxiv a license to display the preprint in perpetuity. It is made available under aCC-BY 4.0 International license.

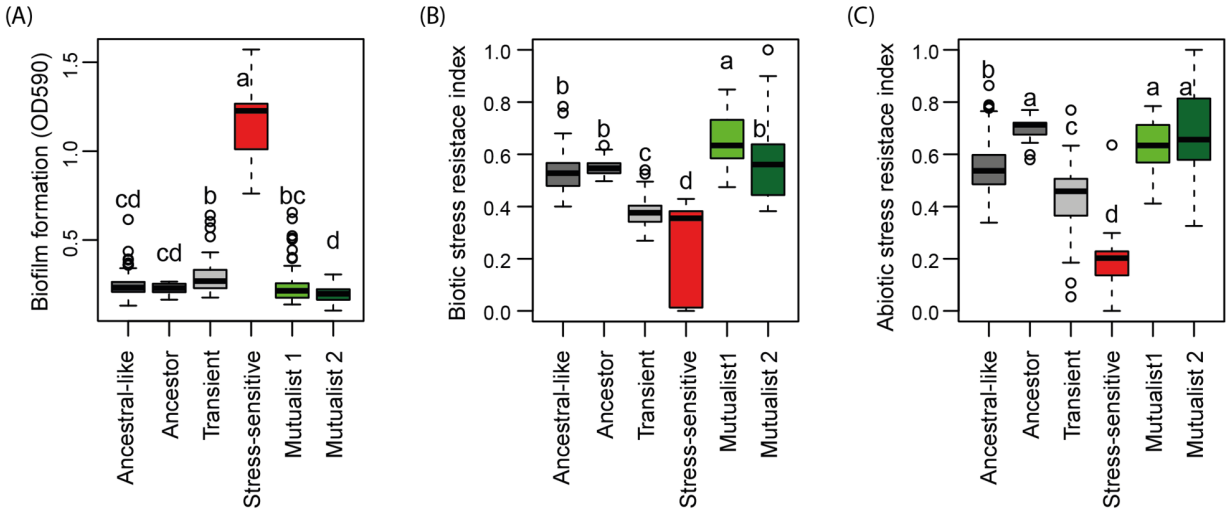

Figure S4. Comparing biofilm formation, biotic and abiotic stress resistance of ancestral and evolved *Pseudomonas protegens* CHA0 isolates. In total, we characterized 16 ancestral, 119 ancestral-like, 11 stress-sensitive, 37 mutualist 1, 31 mutualist 2 and 41 transient isolates (Supplementary dataset 1). Panels A to C show biofilm formation, biotic stress resistance index (normalised PC1 of combined ability to grow in the presence of sub lethal doses of the antibiotics streptomycin, tetracycline and penicillin) and abiotic stress resistance index (normalised first principal component of combined ability of each isolate to grow under oxidative stress, water potential stress and salt stress) respectively. Statistical testing was carried out using ANOVA. Different letters indicate significant differences based on a Tukey HSD test (α=0.05).

bioRxiv preprint doi: https://doi.org/10.1101/2020.12.07.414607; this version posted December 7, 2020. The copyright holder for this preprint (which was not certified by peer review) is the author/funder, who has granted bioRxiv a license to display the preprint in perpetuity. It is made available under aCC-BY 4.0 International license.

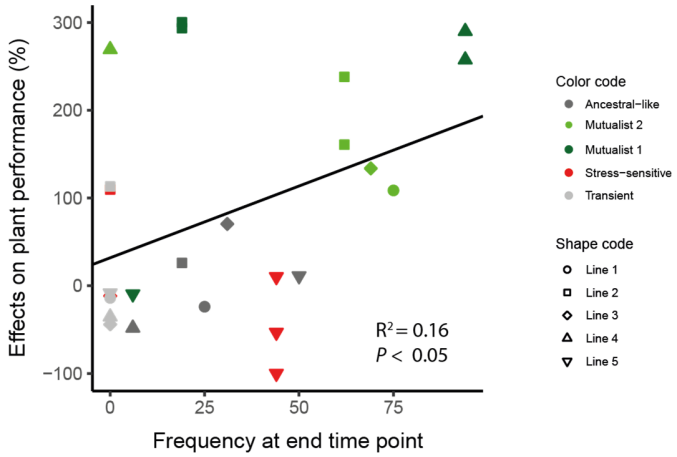

Figure S5. Positive relationship between phenotype frequency at the end of the selection experiment and isolate effect on the plant performance. Five representative bacterial isolates from each phenotype in addition to the ancestor were selected to measure their effects on *Arabidopsis thaliana* growth in terms of combined 'Plant performance' index (30 isolates altogether, each replicate line represented; See Table S2). The y-axis represents the beneficial effect of isolates on plant performance relative to the ancestor. Values on the x-axis show the relative abundance of evolved phenotypes in their respective selection lines at the end of the sixth plant growth cycle (see Figure 1). Colours and shapes represent different phenotypes and selection lines, respectively.

bioRxiv preprint doi: https://doi.org/10.1101/2020.12.07.414607; this version posted December 7, 2020. The copyright holder for this preprint (which was not certified by peer review) is the author/funder, who has granted bioRxiv a license to display the preprint in perpetuity. It is made available under aCC-BY 4.0 International license.

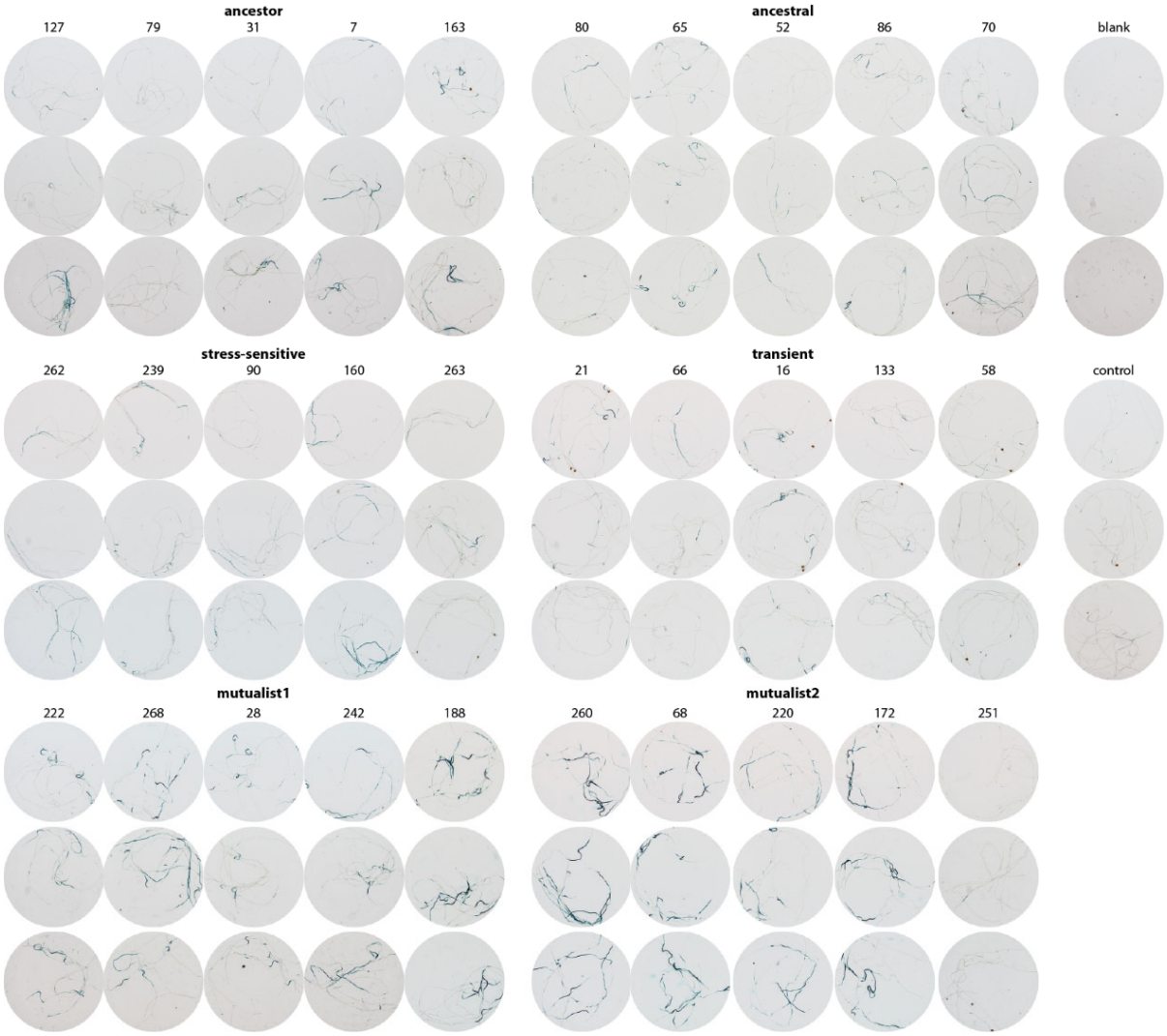

Figure S6. Induction of *MYB72* assayed in a GUS reporter line in *Arabidopsis thaliana* by the ancestor and a subset of evolved *Pseudomonas protegens* CHA0 isolates. GUS staining was performed at 2 days after bacterial inoculation (n = 3 biological plant replicates, each containing 5 to 6 seedlings). See Table S2 for detailed information of the isolates.

bioRxiv preprint doi: https://doi.org/10.1101/2020.12.07.414607; this version posted December 7, 2020. The copyright holder for this preprint (which was not certified by peer review) is the author/funder, who has granted bioRxiv a license to display the preprint in perpetuity. It is made available under aCC-BY 4.0 International license.

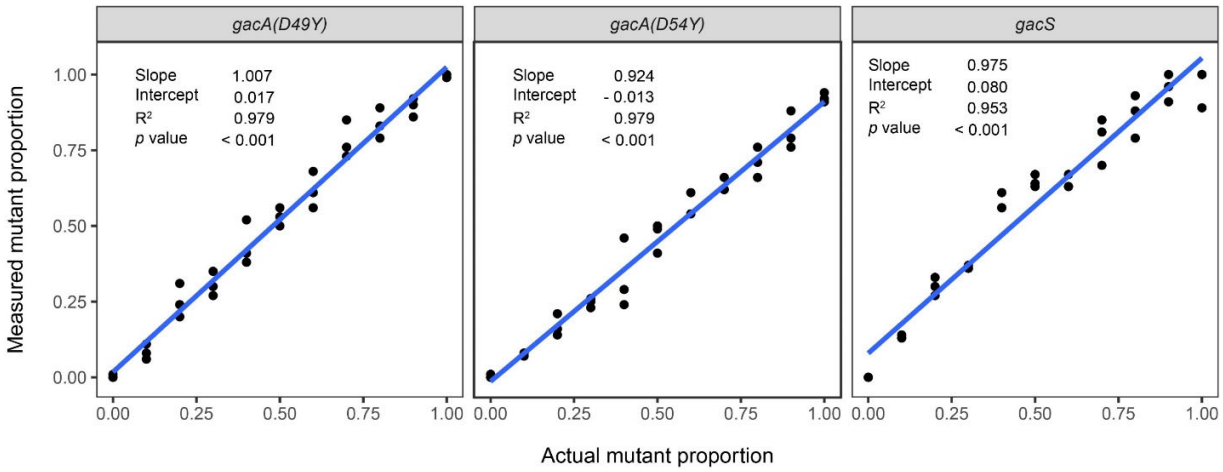

Figure S7 Standard curves of measured mutant versus ancestor proportion as a function of the actual proportion, using series of mixed samples with known proportions (0%, 10%, 20%, 30%, 40%, 50%, 60%, 70%, 80%, 90% and 100% of mutant templates). Relative densities of mutant *gacA*^{D49Y}, *gacA*^{D54Y}, and *gacS*^{G27D} were measured by PCR-based high-resolution melting profile (RQ-HRM) analysis. Measurements for each sample were done in triplicate. In each plot, the black dots represent the measurements, the blue fit line was generated based on linear regression model.

bioRxiv preprint doi: https://doi.org/10.1101/2020.12.07.414607; this version posted December 7, 2020. The copyright holder for this preprint (which was not certified by peer review) is the author/funder, who has granted bioRxiv a license to display the preprint in perpetuity. It is made available under aCC-BY 4.0 International license.

946 **Table S1.** *In vitro* measurement of different aspects of bacterial life-history traits, including
947 bacterial growth, tolerance to diverse abiotic and biotic stresses, production (or activity) of
948 bioactive compounds and antimicrobial activity. In total, 14 different phenotypic traits were
949 measured for 256 *Pseudomonas protegens* CHA0 isolates in this study including 16 isolated
950 isolates of ancestor.

Aspects of life-history traits	**Details of measured traits**
Bacterial growth yield	Bacterial growth yield in King's medium B
Stress tolerance	Growth yield under abiotic stresses: oxidative stress, water potential stress, salt stress Growth yield under biotic stresses (antibiotics): streptomycin stress, tetracycline stress, penicillin stress
Production (or activity) of bioactive compounds	IAA (auxin) production, siderophore activity, quorum sensing (TSO) activity, proteolytic activity, biofilm formation
Antimicrobial activity	Antifungal activity*:* *Verticillium dahliae* Antibacterial activity: *Ralstonia solanacearum*

951

bioRxiv preprint doi: https://doi.org/10.1101/2020.12.07.414607; this version posted December 7, 2020. The copyright holder for this preprint (which was not certified by peer review) is the author/funder, who has granted bioRxiv a license to display the preprint in perpetuity. It is made available under aCC-BY 4.0 International license.

952 **Table S2**. Description of 5 ancestral and 25 evolved *Pseudomonas protegens* CHA0 isolates, which
953 were included to phenotyping and genotyping assays. "Sample ID" is the unique identifier of each
954 isolate and five isolates were selected from each phenotype class. The "Plant cycle" column refers
955 to the plant growth cycle from which the isolate was collected (see Figure S1) and the "Replicate"
956 column refers to the independent plant replicate selection line. Mutated genes were identified using
957 whole genome re-sequencing. On average, each evolved isolate encompassed 2-3 mutations
958 relative to the ancestral sequence that are typically non-synonymous in nature, *i.e.* they directly
959 affect predicted protein sequence and/or protein length. The same Sample ID superscript numbers
960 shown on bold (133 and 242, 66 and 222, 28 and 220) indicate paired samples used in relative
961 competition assays presented in Figure 5.
962

Phenotype	**Sample ID**	**Plant cycle**	**Replicate**	**Genotype**
Ancestor	7	0	Ancestor	_
Ancestor	31	0	Ancestor	_
Ancestor	79	0	Ancestor	_
Ancestor	127	0	Ancestor	_
Ancestor	163	0	Ancestor	_
Ancestral-like	52	4	Line 2	*galE*^{V32M}
Ancestral-like	65	2	Line 3	_
Ancestral-like	70	4	Line 5	_
Ancestral-like	80	4	Line 4	_
Ancestral-like	86	4	Line 1	*oafA*^{Y335X} · *RS17350*$^{A77A.fsX14}$ · *wbpM*^{G79R}
Stress-sensitive	90	4	Line 3	*nlpD*^{Q197P}
Stress-sensitive	160	4	Line 2	*galE*^{V32M} · *accC*^{E413K} · *yvaQ2*$^{-9G>T}$
Stress-sensitive	239	6	Line 5	*rpoS*^{Q65X} · *tetR*^{Y127X}
Stress-sensitive	262	6	Line 5	*rpoS*^{Q65X}
Stress-sensitive	263	6	Line 5	*rpoS*^{Q65X}
Mutualist 1	**28**^{2}	4	Line 2	*galE*^{V32M} · *accC*^{E413K}
Mutualist 1	188	4	Line 4	*gacA*$^{-40T>A}$
Mutualist 1	**222**^{3}	6	Line 3	*oafA*$^{K338S.fsX18}$ · *gacS*^{G27D}

bioRxiv preprint doi: https://doi.org/10.1101/2020.12.07.414607; this version posted December 7, 2020. The copyright holder for this preprint (which was not certified by peer review) is the author/funder, who has granted bioRxiv a license to display the preprint in perpetuity. It is made available under aCC-BY 4.0 International license.

Mutualist 1	**242**[1]	6	Line 1	*oafA*^{Y335X} · *RS17350*$^{A77A.fsX14}$ · *gacA*^{D49Y}
Mutualist 1	268	6	Line 2	*galE*^{V32M} · *accC*^{E413K} · *gacA*^{G97S} · *mraZ*$^{-211A>G}$
Mutualist 2	68	4	Line 4	*gacA*$^{-40T>A}$ · *RS11820*$^{33C>T}$
Mutualist 2	172	4	Line 2	*gacA*^{Y183S}
Mutualist 2	**220**[2]	6	Line 2	*galE*^{V32M} · *accC*^{E413K} · *gacA*^{D54Y}
Mutualist 2	251	6	Line 5	*fleQ*^{R320Q}
Mutualist 2	260	6	Line 4	*gacA*^{E38X} · *RS11785*^{S256C} · *flhA*$^{H393Q.fsX15}$
Transient	16	4	Line 2	*galE*^{V32M} · *accC*^{E413K}
Transient	21	2	Line 4	*hult*$^{786C>T}$
Transient	58	4	Line 5	_
Transient	**66**[3]	4	Line 3	*oafA*$^{K338S.fsX18}$
Transient	**133**[1]	2	Line 1	*oafA*^{Y335X} · *RS17350*$^{A77A.fsX14}$

Note: X, represents a stop codon (at its relative position in case of a shifted frame); fs, frame shift; sequence change positions are relative to the cDNA.

966 **Table S3.** Overview of the affected genes that are identified in the 25 evolved *Pseudomonas protegens* CHA0 isolates (See Table S2).

Gene	***Product***	***Locus tag***	***DNA change***	***Effect***
accC	Biotin carboxylase, acetyl-CoA carboxylase	PFLCHA0_RS03400	c.1237 G>A	p.E413K
flhA	Flagellar biosynthesis protein FlhA	PFLCHA0_RS08490	c.1154 T deleted	early stop
gacA	Response regulator GacA	PFLCHA0_RS17965	c.548 A>C	p.Y183S
gacA	Response regulator GacA	PFLCHA0_RS17965	c.289 G>A	p.G97S
gacA	Response regulator GacA	PFLCHA0_RS17965	c.160 G>T	p.D54Y
gacA	Response regulator GacA	PFLCHA0_RS17965	c.145 G>T	p.D49Y
gacA	Response regulator GacA	PFLCHA0_RS17965	c.112 G>T	p.E38*
gacA	Response regulator GacA	PFLCHA0_RS17965	-40 T>A	promoter
galE	UDP-glucose 4-epimerase	PFLCHA0_RS09920	c.94 G>A	p.V32M
RS11785	LysR family transcriptional regulator	PFLCHA0_RS11785	c.766 A>T	p.S256C
hutI	Imidazolonepropionase	PFLCHA0_RS02080	c.786 C>T	synonymous
RS11820	PaaI family thioesterase	PFLCHA0_RS11820	c.33 C>T	synonymous
yvaQ2	Metyl-accepting chemotaxis protein	PFLCHA0_RS13000	-9bp G>T	promoter
mraZ	Transcriptional regulator mraZ	PFLCHA0_RS25175	-211bp A>G	promoter
nlpD	Lipoprotein nlpD/lppB/LysM domain-containing protein	PFLCHA0_RS31060	c.590 A>C	p.Q197P
fleQ	Sigma-54-dependent Fis family transcriptional regulator	PFLCHA0_RS08340	c.959 G>A	p.R320Q
oafA	O-acetyltransferase OatA	PFLCHA0_RS09890	c.1005 C>A	p.Y335*
oafA	O-acetyltransferase OatA	PFLCHA0_RS09890	c.1009 A deleted	early stop

bioRxiv preprint doi: https://doi.org/10.1101/2020.12.07.414607; this version posted December 7, 2020. The copyright holder for this preprint (which was not certified by peer review) is the author/funder, who has granted bioRxiv a license to display the preprint in perpetuity. It is made available under aCC-BY 4.0 International license.

wbpM	Polysaccharide biosynthesis protein/NDP-sugar epimerase	PFLCHA0_RS21855	c.235 G>C	p.G79R
rpoS	RNA polymerase sigma factor RpoS	PFLCHA0_RS06125	c.193 C>T	p.Q65*
RS17350	Methyltransferase domain-containing protein	PFLCHA0_RS17350	c.116 C deleted	early stop

967

bioRxiv preprint doi: https://doi.org/10.1101/2020.12.07.414607; this version posted December 7, 2020. The copyright holder for this preprint (which was not certified by peer review) is the author/funder, who has granted bioRxiv a license to display the preprint in perpetuity. It is made available under aCC-BY 4.0 International license.

Table S4 Primers and probes used for high-resolution melting (HRM) analysis. For the two *gacA* mutants the same set of primers was used. Underlined bases indicate the position of the single nucleotide point (SNP) mutations within the probe sequences. ΔTm (°C) indicates the melting temperature difference between WT-probe duplex and mutant-probe duplex.

Target gene	Strain ID	SNP locus	Forward primer (excess)	Reverse primer (limiting)	Amplicon size	Probe sequence	Probe length	Target strand	Perfect match/ mismatch	$_{\Delta}$Tm (°C)
gacA^{D49Y}	242	145G>T	5'-ATCGATGGCCTGCAAGTAGT-3'	5'-CGGGTAGGAAAGGGATCTTC-3'	206 bp	5'-CATCAGGACCACATCGGGCTTCAGCTCCCG-/C3/3'	30nt	WT	G::C / T::C	5.31
gacA^{D54Y}	220	160G>T				5'-TGGCATCTTGACGTCCATCAGGACCACATC-/C3/3'	30nt	WT	G::C / T::C	4.92
gacS^{G27D}	222	80G>A	5'-GCGTACTGTTGCTGACCTTG-3'	5'-AGCATCTGGGTGTTGTGGTT-3'	178bp	5'-AGGTGAAGTAGCCGCCCAGCACCAAAGCCA-/C3/3'	30nt	WT	G::C / A::C	4.83

bioRxiv preprint doi: https://doi.org/10.1101/2020.12.07.414607; this version posted December 7, 2020. The copyright holder for this preprint (which was not certified by peer review) is the author/funder, who has granted bioRxiv a license to display the preprint in perpetuity. It is made available under aCC-BY 4.0 International license.

Supplementary dataset 1: Sheet 1: Summary table for the set of fourteen phenotypic traits for the 256 characterised isolates used for K-mean clustering. Sheet 2: Carbon use data for the 256 characterised isolates. In both sheets, each line corresponds to one isolate and each column to one specific trait. See material and methods for a detailled description of experimental procedures.

Supplementary dataset 2: Sheet 1: Recapitulation of the origin (replicate line), time point and phenotype of each of the 30 isolates tested in details for their interactions with the host plant. Sheet 2: Summary table for interactions between each of the 30 isolates tested for plant growth, including effect on plant performance and induced GUS expression. Sheet 3: Scopoletin sensitivity. See material and methods for a detailled description of experimental procedures.

bioRxiv preprint doi: https://doi.org/10.1101/2020.12.07.414607; this version posted December 7, 2020. The copyright holder for this preprint (which was not certified by peer review) is the author/funder, who has granted bioRxiv a license to display the preprint in perpetuity. It is made available under aCC-BY 4.0 International license.